AIAA 2003-0925

F/A-18C TO E WING MORPHING STUDY FOR THE ABRUPT WING STALL PROGRAM

Bradford E. Green
NAVAIR
Patuxent River, MD

James D. Ott
Combustion Research and Flow Technology, Inc.
Dublin, PA

41st AIAA Aerospace Sciences Meeting & Exhibit
6-9 January 2003
Reno, Nevada

Report Documentation Page

Form Approved
OMB No. 0704-0188

1. REPORT DATE	2. REPORT TYPE	3. DATES COVERED
JAN 2003		**00-01-2003 to 00-01-2003**

4. TITLE AND SUBTITLE	5a. CONTRACT NUMBER
F/A-18C to E Wing Morphing Study for the Abrupt Wing Stall Program	5b. GRANT NUMBER
	5c. PROGRAM ELEMENT NUMBER
6. AUTHOR(S)	5d. PROJECT NUMBER
	5e. TASK NUMBER
	5f. WORK UNIT NUMBER
7. PERFORMING ORGANIZATION NAME(S) AND ADDRESS(ES) **Combustion Research and Flow Technology Inc (CRAFT Tech),6210 Keller's Church Road,Pipersville,PA,18947**	8. PERFORMING ORGANIZATION REPORT NUMBER
9. SPONSORING/MONITORING AGENCY NAME(S) AND ADDRESS(ES)	10. SPONSOR/MONITOR'S ACRONYM(S)
	11. SPONSOR/MONITOR'S REPORT NUMBER(S)

12. DISTRIBUTION/AVAILABILITY STATEMENT
Approved for public release; distribution unlimited

13. SUPPLEMENTARY NOTES
The original document contains color images.

14. ABSTRACT

15. SUBJECT TERMS

16. SECURITY CLASSIFICATION OF:			17. LIMITATION OF ABSTRACT	18. NUMBER OF PAGES	19a. NAME OF RESPONSIBLE PERSON
a. REPORT	b. ABSTRACT	c. THIS PAGE			
unclassified	**unclassified**	**unclassified**		**31**	

Standard Form 298 (Rev. 8-98)
Prescribed by ANSI Std Z39-18

F/A-18C TO E WING MORPHING STUDY FOR THE ABRUPT WING STALL PROGRAM

Bradford E. Green *
NAVAIR
Patuxent River, MD

James D. Ott †
Combustion Research and Flow Technology, Inc. (CRAFT)
Dublin, PA

Abstract

In an effort to determine the impact of various wing parameters on the abrupt wing stall phenomenon encountered by the pre-production F/A-18E, various characteristics of the F/A-18C wing were modified to reflect the design changes incorporated into the F/A-18E wing. The parameters evaluated during this study included thickness, camber, twist, leading-edge radius, leading-edge flap-chord ratio and the addition of a leading-edge snag. The wing parameters were modified independently and then in combination to determine their impact on the abrupt stall. Several potential computational Figures of Merit were evaluated to determine their utility for the prediction of an abrupt wing stall. One of the most promising Figures of Merit for indicating the onset of an abrupt stall was found to be the wing-root bending-moment coefficient. Using this Figure of Merit, it was determined that the incorporation of a leading-edge snag, the reduction of leading-edge flap-chord ratio and the elimination of camber are the likely contributors to the abrupt stall phenomenon encountered by the aircraft.

Nomenclature

a_∞	free-stream speed of sound, ft/s
b	wing span, ft
c	chord of wing airfoil section, ft
C_D	aircraft drag coefficient, $D/(q_\infty S)$
C_L	aircraft lift coefficient, $L/(q_\infty S)$
C_p	static pressure coefficient, $(P-P_\infty)/(q_\infty)$
C_{WB}	wing-root bending-moment coefficient
c_l	sectional lift coefficient, $l/(q_\infty c)$
D	drag on aircraft, lb
L	lift on aircraft, lb
l	wing sectional lift, lb/ft
M	free-stream Mach number, U_∞ / a_∞
P	static pressure, lb/ft^2
q_∞	dynamic pressure, $(0.5\rho_\infty U_\infty^2)$, lb/ft^2
Re	Reynolds number, $(\rho_\infty U_\infty c_{mac})/\mu_\infty$
S	wing reference area, ft^2
U_∞	free-stream velocity, ft/s
x	chordwise distance along wing, ft
y	spanwise distance along wing, ft

Greek

α	angle of attack, degrees
ρ_∞	free-stream density, slugs/ft^3
μ_∞	free-stream dynamic viscosity, slugs/ft-s

Subscripts

mac	mean aerodynamic chord
ref	reference
root	wing root
tip	wing tip
∞	free-stream

---

* Aerospace Engineer, Member AIAA
† Aerospace Engineer, Member AIAA

Acronyms

AEDC	Arnold Engineering Development Center
AoA	Angle of Attack
AWS	Abrupt Wing Stall
CFD	Computational Fluid Dynamics
EMD	Engineering and Manufacturing Development
FOM	Figure of Merit
LEX	Leading-Edge Extension
MAC	Mean Aerodynamic Chord
PWT	Propulsion Wind Tunnel
WRBM	Wing-Root Bending-Moment

Introduction

During the Engineering and Manufacturing Development (EMD) phase of the F/A-18E/F program, pre-production aircraft encountered an uncommanded, abrupt rolling motion during transonic maneuvering conditions. Commonly referred to as abrupt wing stall (AWS), this phenomenon occurs when there is a loss in roll damping or when the amount of flow separation on the upper surface of the wings increases rapidly and asymmetrically. A rolling moment results from the difference in lift that is generated between the two wings. Abrupt stall degrades the tracking capability of the aircraft and causes safety concerns if it occurs at low altitudes.[1]

Modifications of the automatic leading-edge flap schedule and the addition of a porous surface at the wing fold solved the abrupt stall problem on the F/A-18E/F and were incorporated into the production versions of the aircraft. As a result of the modifications, the F/A-18E/F's being delivered to the fleet are no longer susceptible to AWS. On the recommendation of a high level panel that over viewed the technical problems encountered in the early development program, the AWS program was formed to obtain a better understanding of the causes of abrupt stall.[2] The AWS program is a national team composed of the Navy, NASA, Air Force and several universities. The research presented in this paper was funded through the AWS program.

The reader is cautioned that references to the F/A-18E configuration herein are to the pre-production configuration without the wing modifications. In particular, the current study was for an aircraft without porosity.

There are significant differences in the wing characteristics between the F/A-18C and the F/A-18E. During the development of the F/A-18E, changes were made to the wing by modifying the thickness, camber, twist, leading-edge radius, leading-edge flap-chord ratio and adding a leading-edge snag. The differences in these wing parameters between the F/A-18C and the F/A-18E are shown in Table 1. Since the F/A-18C does not experience abrupt stall within its flight envelope, the goal of this research was to determine which of these wing parameters contributed to the abrupt stall phenomenon initially encountered by the F/A-18E.

Computational Fluid Dynamics (CFD) was used as the tool to accomplish this goal. To determine the effect of each of the wing parameters listed in Table 1, the grid of the F/A-18C was modified or "morphed" to reflect the changes made to these parameters when designing the F/A-18E. For example, to determine the effect of twist on abrupt stall, the twist was removed from the F/A-18C grid to form a "morphed" grid. The twist was removed from the F/A-18C grid since, as shown in Table 1, the F/A-18C wing has twist while the F/A-18E wing does not. The parameters listed in Table 1 were modified independently and then in combination.

Table 1. Comparison of wing parameters on the F/A-18C and F/A-18E

Wing Parameter	F/A-18C	F/A-18E
Thickness	3.5% to 5.0% chord	3.8% to 6.2% chord
Camber	0.6% chord	No Camber
Twist	4° Outboard Twist	No Twist
Snag	No Snag	LE Snag
LE radius	0.08 to 0.31 inches	0.04 inches
LE flap-chord ratio	20% chord	11.3% to 18.1% chord

After analyzing each of the configurations at transonic speeds, the wing-root bending-moment (WRBM) coefficient was plotted as a function of angle of attack (AoA). Based on the Figures of Merit developed during the AWS program[3], abrupt stall can occur when the slope of the coefficient of WRBM curve changes sign. The AoA at which the slope changes sign is of particular importance. If, for any of the morphed configurations, the slope of the WRBM curve changes sign at a lower AoA than it does for the F/A-18C, then this indicates that the particular wing parameter or parameters being modified may be contributing to abrupt stall.

In the following sections, the CFD flow solver and the F/A-18C grid will be discussed. Next, the F/A-18C results from CFD will be compared to the results from the wind-tunnel experiment. Then, the WRBM Figure of Merit will be discussed as well as the methodology used to accomplish the goal of this research. The CFD analysis of the F/A-18C grid will be presented prior to discussing the results of the morphing study. In the last section, the concluding remarks will be presented.

Discussion of the CFD Flow Solver

The WIND flow solver[4] was used to obtain the flow solution on the F/A-18C configuration and all of the morphed configurations studied during this project. This flow solver is an extension of the NASTD code, which was developed by McDonnell Douglas Aerospace-East. WIND solves the Reynolds-averaged Navier-Stokes equations in conservative form using second-order-accurate finite differences on structured, multi-zonal computational grids. The explicit terms are computed using either upwind or central difference. The implicit terms are computed using either an approximately factored or four-stage Runge-Kutta scheme.

Several turbulence models are available within WIND. Some of these models include Cebeci-Smith, Baldwin-Lomax, Spalart-Allmaras and Menter's SST model. Menter's SST model[5] was used during this research, since it was determined early in the AWS program that the solutions on the F/A-18E using Menter's SST correlated better with wind-tunnel results than did the results using Spalart-Allmaras.[2]

F/A-18C Grid

The structured, overset F/A-18C grid is shown in Figure 1. The grid is comprised of 79 blocks and has approximately 13.9 million points. To reduce the size of the grid, only half of the configuration is modeled using a plane of symmetry along the fuselage centerline. The horizontal and vertical tails are not represented in the grid, since it was anticipated that they would have little impact on the abrupt stall phenomenon encountered by the F/A-18E.

In the grid, the leading- and trailing-edge flaps are deflected to 6 and 8 degrees, respectively, while the aileron is not deflected. This is referred to as a 6°/8°/0° flap setting. A missile launcher and a Sidewinder missile are attached to the wing tip.

The WIND flow solver required 900 MBytes of memory on Silicon Graphics Octanes and Origin 2000/3000/3800 machines. Each solution required approximately 6000 CPU-hours to complete.

Comparison with Wind-Tunnel Experiment

The F/A-18C grid was analyzed at Mach 0.8 and 0.9 at a Reynolds number of 2.07 million based on the mean aerodynamic chord (MAC) for several AoA and the results were compared to the wind-tunnel data obtained from the 4-Foot Transonic Propulsion Wind Tunnel (PWT) at the Arnold Engineering Development Center (AEDC). A Reynolds number of 2.07 million corresponds to the wind-tunnel Reynolds number of 3 million/ft for a 6% scale model. In Figure 2, the lift and drag coefficients from CFD are compared to the wind-tunnel data obtained at the AEDC. In general, the lift and drag coefficients from CFD compare very well with the wind tunnel data. The lift from CFD does slightly over-predict the wind tunnel data. This over-prediction can probably be explained by the fact that the wind-tunnel model had horizontal and vertical tails, while the CFD

grid did not. The wind tunnel data shown in Figure 2 was obtained while the horizontal tail deflection angle was 0 degrees.

Oil flow images on the wing upper surface were also obtained during the AEDC wind tunnel test. In general, the surface-restricted particle traces from CFD compare well with the oil flow images from the wind tunnel experiment. Figure 3 shows two comparisons between wind tunnel oil flow images and surface-restricted particle traces from CFD at Mach 0.8. At an AoA of 7 degrees, both the wind tunnel oil flow and CFD particle traces predict flow separation and reattachment on the wing box. At an AoA of 11 degrees, both the oil flow and CFD surface-restricted particle traces indicate that flow separation has reached the leading edge.

The correlation of the lift, drag and oil flow images between CFD and the wind tunnel experiment indicate that the grid and flow solver are adequate for accurately predicting the flow over the F/A-18C.

Wing-Root Bending-Moment Coefficient as a Figure of Merit

The WRBM coefficient was utilized as a Figure of Merit (FOM) for identifying AWS.[3] The WRBM is calculated using the equation

$$WRBM = \int_{y_{root}}^{y_{tip}} l(y - y_{ref})dy$$

on the wing of the aircraft. In this equation, y_{ref} was taken to be at the interface between the wing and the leading-edge extension (LEX) of the F/A-18C. The WRBM coefficient is then obtained using the equation

$$C_{WB} = \frac{WRBM}{q_\infty S_{ref} b_{ref}}$$

Based on correlation between wind tunnel and flight tests, abrupt stall can occur when the slope of the WRBM versus AoA curve changes sign. Abrupt stall, however, is not guaranteed to occur when the slope of the WRBM changes sign. The change in sign could also occur with no significant lateral activity being present. The change in sign suggests that further testing is necessary to determine if there is an unacceptable lateral problem.

Since the change in sign of the slope of the WRBM curve can indicate the onset of the abrupt stall, the AoA where the slope changes sign will be referred to as the onset AoA. The onset AoA indicates the lower boundary of an AWS region of interest, in which abrupt stall could occur. The AWS region of interest extends approximately from the onset AoA to an AoA where the slope of the WRBM starts increasing again.

In Figure 4, the WRBM coefficient is plotted as a function of AoA for the F/A-18C at Mach 0.8 and 0.9 and the F/A-18E at Mach 0.9. It can be seen in the figure that the onset AoA for the F/A-18C is 10 degrees at Mach 0.8 and 11 degrees at Mach 0.9. Although the slope of the WRBM curve changes sign for the F/A-18C with 6°/8°/0° flaps, the flaps are not on schedule at 10 and 11 degrees AoA. As a result, the F/A-18C does not experience abrupt stall within its flight envelope.

The pre-production F/A-18E, however, did experience abrupt stall. The WRBM coefficient in Figure 4 for the F/A-18E with 6°/8°/4° flaps changes sign at 7.5 degrees. Since the 6°/8°/4° flaps are nearly on schedule for the pre-production aircraft at 7.5 degrees AoA, the abrupt stall occurred within the flight envelope of the aircraft.

When analyzing the WRBM coefficient to determine if the slope changes sign, smaller increments in AoA may be necessary. In Figure 5, the initial and refined WRBM curves are shown for two cases. For the first case, which is illustrated using the plots at the top, the initial WRBM curve was obtained using AoA increments of 1 degree. Using increments of 1 degree does not clearly resolve a change in sign of the slope. It appears, though, that a change in sign of the slope could occur between 10 and 11 degrees AoA. As a result, the 10.5 degree AoA case was analyzed and used to create the refined WRBM curve shown on the top, right-hand side of the figure. This plot clearly shows that the slope changes sign at an AoA of 10 degrees.

The bottom two plots in Figure 5 are used to illustrate the second case where a smaller AoA increment could be helpful. The initial WRBM curve in the lower, left-hand plot was generated using AoA increments of 1 degree. The slope of

this curve changes sign at 7 degrees AoA. When the curve is refined by calculating the flow at 7.5 degrees AoA, the slope changes sign at 7.5 degrees, as shown in the plot on the lower, right-hand side of Figure 5. In addition, the refined curve has an extremely different character since the peak of the curve where the slope changes sign is significantly larger.

The lift-curve slope was also considered as a potential FOM during the AWS program.[3] Specifically, the location of the break in the lift versus AoA curve was viewed as a possible indicator of abrupt stall. In Figure 6, the lift and WRBM coefficients are plotted as a function of AoA for the F/A-18C at Mach 0.8 and 0.9. While the slope of the WRBM coefficient changes sign at 10 and 11 degrees for Mach 0.8 and 0.9, respectively, the slope of the lift coefficient changes sign only at 10 degrees for Mach 0.8. At Mach 0.9, it is difficult to determine where the lift versus AoA curve breaks. As a result, the change in sign of the slope of the WRBM curve was used as the FOM for this study.

Methodology

In an effort to determine their impact on abrupt stall, the wing parameters listed in Table 1 were evaluated by modifying the F/A-18C wing to reflect the changes that were made to the wing when designing the F/A-18E. This process of modifying the wing parameters on the F/A-18C wing is referred to as "morphing". Eleven different morphing configurations, which are shown in Figure 7, were used to determine if the six wing parameters were contributing to the abrupt stall. For the first six morphing cases shown in Figure 7, the F/A-18C was modified to reflect the change made for the specific wing parameter. For example, morphing case #4 in Figure 7 represents the F/A-18C with an untwisted wing. While removing the twist from the wing, the other wing parameters shown in Table 1 were unchanged. The twist was removed from the F/A-18C wing since the F/A-18E wing is untwisted, as shown in Table 1.

Morphing cases 7 through 11 in Figure 7 represent cases where two wing parameters were modified simultaneously. Specifically, these cases show the effect of the latter five wing parameters on a wing with a snag. For example, morphing case #8 represents a configuration where a snag was added to the F/A-18C wing while at the same time the camber was removed from the wing. The camber was removed from the wing since the F/A-18E wing is uncambered.

After creating the new grids with the desired changes in wing parameters, solutions were generated at Mach 0.8 and 0.9 for several AoA's. The WRBM coefficient was then plotted as a function of AoA to determine which wing parameters were having an effect on abrupt stall.

From Figure 4, one can see the changes in WRBM coefficient that indicate that a particular wing parameter is contributing to abrupt stall. Since the F/A-18C wing is being morphed to mimic an F/A-18E wing, one should expect that wing parameters contributing to abrupt stall would move the onset AoA in the WRBM curve from the F/A-18C toward the F/A-18E. In particular, the AoA at which the slope changes sign will be reduced from 10 and 11 degrees at Mach 0.8 and Mach 0.9 to approximately 7.5 degrees AoA or less.

To mimic the flap settings for the F/A-18C grid that was analyzed and compared to wind-tunnel data, each of the morphing configurations were analyzed with 6°/8°/0° flaps. In Figure 4 and throughout this paper, the F/A-18C with 6°/8°/0° flaps was compared to the F/A-18E with 6°/8°/4° flaps. The only difference between these two flap settings is that the aileron is not deflected on the F/A-18C, while the aileron is deflected –4 degrees on the F/A-18E. This difference in flap settings is probably not contributing to the significant difference in the AWS characteristics seen between the two aircraft, since unpublished Veridian wind-tunnel data indicates that abrupt wing stall is more sensitive to the leading-edge flap setting than it is to the trailing-edge flap and aileron settings.

Before presenting the results of the morphing study, the results of the analysis of the F/A-18C will be presented.

Analysis of the F/A-18C

In this section, the baseline F/A-18C results will be discussed. In Figures 8 and 9, the pressure coefficients, surface-restricted particle traces and regions of off-body flow reversal on the upper surface of the wing are shown for several AoA at Mach 0.8 and 0.9. The areas above the wing covered in red indicate the regions of flow reversal. As expected, for both Mach numbers the flow separation moves toward the leading edge as the AoA is increased. Since abrupt stall occurs when the amount of flow separation increases rapidly with AoA, analyzing the regions of flow separation and how they change with increasing AoA is important.

In Figure 10, the sectional lift coefficient and its derivative with AoA are plotted as a function of spanwise location for the F/A-18C at Mach 0.8 and 0.9. It can be seen from the figure that the sectional lift increases over the span until 11 and 12 degrees AoA at Mach 0.8 and 0.9, respectively. The discontinuity in the F/A-18C sectional lift plots near 2y/b=0.67 is caused by the different deflections between the trailing-edge flap and the aileron. Recall that the WRBM coefficient for the F/A-18C changed sign at 10 and 11 degrees for Mach 0.8 and 0.9, respectively. This is consistent with the loss in lift that appears in Figure 10.

Plots of $dc_l/d\alpha$ yielded valuable information during this research. These plots give insight into the location on the span where lift is being lost. This can help tremendously when determining the factors that are contributing to abrupt stall. Furthermore, there is a good correlation between the AoA where the largest amount of lift is lost on the $dc_l/d\alpha$ plots and the onset AoA from the WRBM curves.

Results

In this section, the results from the morphing study will be presented. In each of the six subsections that follow, the results from a particular wing parameter will be discussed and conclusions will be drawn about the effect of the wing parameter on abrupt stall.

To help compare the cases, the difference between the onset AoA for each of the morphing configurations and the baseline F/A-18C for Mach 0.8 and 0.9 is shown in Table 2. As an example, the first case listed in the table represents the F/A-18C with reduced leading-edge radius. In general, as one goes from the top to the bottom of the table, the difference between the onset AoA of the morphed configuration and the F/A-18C becomes larger.

Table 2. Difference in onset AoA between morphing configurations and the F/A-18C

	Mach 0.8	Mach 0.9
LE Radius	0	0
Twist	-1	0
Camber	-1.5	0
11.3% LE Flap-Chord Ratio	-1	-1
Thickness	-2.5 & 0	-1
Snag	-2	-2
Snag, Thickness	-2	-1
Snag, Twist	-2	-2
Snag, LE Radius	-2	-2
Snag, Camber	-2.5	-2.5
Snag with Tapered LE Flap	-3.5	-3.2

Snag

During the design of the F/A-18E wing, a leading-edge snag was added to the wing to improve the high-lift performance of the aircraft at low speeds. There is no leading-edge snag on the F/A-18C.

During this research, a leading-edge snag was added to the F/A-18C wing to determine its effect on abrupt stall. This case corresponds to morphing

case #1 in Figure 7. The planform of the F/A-18C wing with a snag is compared to that of the F/A-18C wing in Figure 11. In this figure, the baseline F/A-18C wing is shown in the upper-left corner, while the F/A-18C wing with a snag is shown in the lower-left corner. The wings are colored to distinguish the leading-edge flap, wing box, trailing-edge flap and aileron.

The snag was placed at the same non-dimensional spanwise location as it is on the F/A-18E. To create the snag, the leading-edge flap of the F/A-18C was extended so that the ratio of the chord length between the airfoil section outboard of the snag and inboard of the snag was identical to that of the F/A-18E. Since the snag was placed near the wing-fold fairing on the F/A-18C, the wing-fold fairing and other protuberances were removed from the wing to simplify the process of adding the snag. With the exception of the wing-fold fairing, the leading-edge flap on the F/A-18C wing was only modified outboard of the snag location.

The results of WRBM coefficient for the F/A-18C and the F/A-18C with a snag are shown in Figure 12. It can be seen in the figure that the addition of a snag changes the WRBM curves significantly. At Mach 0.8, the onset AoA for the configuration with a snag is 8 degrees. This represents a reduction of two degrees in the onset AoA from the F/A-18C. At Mach 0.9, the addition of the leading-edge snag reduces the onset AoA by two degrees from 11 to 9 degrees. A 2-degree reduction in the onset AoA is large and, as a result, the snag is most likely a significant contributor to the abrupt stall initially encountered by the F/A-18E.

The WRBM curves at Mach 0.8 and 0.9 for the F/A-18C with a snag are compared in Figure 13. These curves differ in character, partially because the WRBM curve at Mach 0.8 has a sharper peak where the slope changes sign. The sharper peak at Mach 0.8 is also manifested by a larger loss in lift in the $dc_l/d\alpha$ curves, which are also shown in Figure 13. In each of the $dc_l/d\alpha$ plots, the largest loss in lift corresponds to the onset AoA on the WRBM plots. These results indicate that the $dc_l/d\alpha$ curves are useful for predicting the severity of the abrupt stall, in addition to the AoA where the abrupt stall occurs.

The sectional lift and $dc_l/d\alpha$ are plotted as a function of spanwise location for the F/A-18C and F/A-18C with a snag at Mach 0.9 in Figure 14. The $dc_l/d\alpha$ curves for the F/A-18C with a snag indicate that the largest loss in lift occurs between 9 and 9.5 degrees AoA and is centered near the location of the snag. Furthermore, this loss in lift is greater than the F/A-18C experienced between 11 and 12 degrees AoA.

In Figure 15, the pressures, surface-restricted particle traces and regions of off-body flow reversal on the upper surface of the wing for the F/A-18C and the F/A-18C with a snag are compared at Mach 0.9 for 8, 9 and 10 degrees AoA. In this figure, the F/A-18C wing is shown on the top while the F/A-18C wing with a snag is shown on the bottom. At 8 and 9 degrees AoA, the flow separates at nearly the same location on both wings. However, at 10 degrees AoA the flow separation on the wing with a snag has moved further forward than the separation on the F/A-18C. This rapid, forward movement of the flow separation region for the F/A-18C with a snag between 9 and 10 degrees AoA is causing the slope to change sign in the WRBM in Figure 12 and the loss in lift that occurs in Figure 14.

In Figure 16, the chordwise pressure distribution is plotted just inboard of the snag for several AoA for the F/A-18C and F/A-18C with a snag at Mach 0.9. For the F/A-18C with a snag, the pressure coefficient is more negative at the leading edge and the pressure gradient on the leading-edge flap is more adverse than it is on the F/A-18C. Between 9 and 12 degrees AoA, the shock on the upper surface of the F/A-18C with a snag moves forward more rapidly than it does on the F/A-18C. At 12 degrees AoA, the flow separation has reached the leading edge of the wing with a snag.

As mentioned above, the leading-edge snag is contributing significantly to abrupt stall at both flow conditions considered. The reason that the snag is contributing to abrupt stall is shown in Figures 17 and 18. The particle traces near the snag on the F/A-18C with a snag configuration are shown in Figure 17. As the flow accelerates around the inboard edge of the snag, a region of low pressure is formed on the upper surface of the leading-edge flap inboard of the snag. This region of low pressure causes a steep adverse pressure gradient which separates the flow on the flap

inboard of the snag. The region of reversed flow is shown in red on the right-hand plot in Figure 17. As a result of the adverse pressure gradient and flap separation, the boundary layer thickens and separates earlier on the wing. A typical plot of the contours of boundary layer thickness for the F/A-18C and F/A-18C with a snag is shown in Figure 18. In this figure, the boundary layer becomes thicker as the color changes from blue to red. For the F/A-18C with a snag, the boundary layer starts thickening on the leading-edge flap just inboard of the snag.

Since the addition of a leading-edge snag to the F/A-18C wing reduced the onset AoA by 2 degrees at both Mach 0.8 and 0.9, the camber, thickness, twist, leading-edge radius and leading-edge flap-chord ratio on the F/A-18C were modified independently and then in combination with the leading-edge snag. The results for these five wing parameters in combination with the snag are compared to the results of the F/A-18C with the snag in this section.

Thickness

The effect of thickness on abrupt stall was determined by analyzing two different configurations, as shown in Figure 7. In the first case, the thickness of the F/A-18C wing was increased, as indicated in Table 1. In Figure 19, the WRBM coefficient is shown as a function of AoA for the F/A-18C and the F/A-18C with a thickened wing for Mach 0.8 and 0.9. At Mach 0.8, the slope changes sign at 7.5 and 10 degrees for the thickened wing. The change in sign at 7.5 degrees represents a 2.5-degree reduction in onset AoA from the F/A-18C. At Mach 0.9, the slope changed sign at 10 degrees for the thickened wing. This represents a 1-degree reduction from the F/A-18C.

The F/A-18C with a thickened wing at Mach 0.8 was the only configuration in this study where the slope changed sign in two distinct AoA regions. To test a potential $dc_l/d\alpha$ FOM, the WRBM curve and $dc_l/d\alpha$ for the thickened wing at Mach 0.8 were plotted as a function of spanwise location in Figure 20. This figure indicates that there is a large loss in lift at 7.5 and again at 10 degrees AoA, the two AoA where the slope of the WRBM changes sign. This increases the credibility that $dc_l/d\alpha$ can be used as a FOM.

For the second case, the F/A-18C was modified by adding a leading-edge snag and thickening the wing. The WRBM for this configuration is compared to that of the F/A-18C with a snag at Mach 0.8 and 0.9 in Figure 21. At Mach 0.8, the increase in thickness does not change the onset AoA. At Mach 0.9, however, the onset AoA increases by 1 degree as a result of the increase in wing thickness. This was the only case examined during this study where a change in a wing parameter increased the onset AoA.

Based on these results, thickness does not appear to be contributing to abrupt stall on the F/A-18E.

Camber

Morphing cases 3 and 8 in Figure 7 were used to analyze the effect of camber on abrupt stall. In the first case, the camber was removed from the F/A-18C wing. In the second case, the camber was removed from the F/A-18C wing while also adding a leading-edge snag. The WRBM curves for these cases at Mach 0.8 and 0.9 are shown in Figure 22. The results for the first case are shown in the plots at the top, where the WRBM curves for the F/A-18C with an uncambered wing are compared to that of the F/A-18C. These results indicate that the removal of the camber from the F/A-18C wing reduced the onset AoA by 1.5 degrees at Mach 0.8. The removal of the camber from the wing does not change the onset AoA at Mach 0.9.

The results for the second case are shown in the plots at the bottom of Figure 22. In these plots, the WRBM curves for the F/A-18C with a snag and uncambered wing are compared to those of the F/A-18C with a snag for Mach 0.8 and 0.9. These two plots indicate that removal of the camber from the wing with a snag reduces the onset AoA by 0.5 degree at both Mach numbers.

Based on these results, the removal of the camber from the wing could be a contributing factor to AWS. A possible explanation for the contribution of the camber to abrupt stall can be seen in Figure 23. In this figure, the upper surface pressure contours, surface-restricted particle traces and regions of flow reversal for the F/A-18C with a snag and the F/A-18C with a snag and

uncambered wing are shown at Mach 0.8 for several AoA. In this figure, the 6, 7 and 8 degree uncambered cases appear to be very similar to the 7, 8 and 9 degree cambered cases. This shift in AoA is probably being caused by the increased loading on the leading-edge flap that results from uncambering the flap. The removal of the camber from the flap increases the relative AoA between the mean-camber line of the flap and the oncoming flow.

Twist

The effect of twist on abrupt stall was determined by analyzing two different configurations. These cases are shown as morphing cases 4 and 9 in Figure 7. In the first case, the twist was removed from the F/A-18C wing. In the second case, a leading-edge snag was added to the F/A-18C wing while removing the twist from the wing. The WRBM is shown as a function of AoA for both cases in Figure 24. The two upper plots show the results of the first case, while the two lower plots show the results of the second case. Although removing the twist from the F/A-18C wing reduced the onset AoA by 1 degree at Mach 0.8, the removal of the twist did not shift the onset AoA at Mach 0.9. Furthermore, after adding a snag to the wing, removing the twist did not change the onset AoA at Mach 0.8 or 0.9. These results indicate that the removal of the twist is not contributing to abrupt stall on the F/A-18E.

Leading-Edge Radius

The effect of leading-edge radius on abrupt stall was also investigated in this study. As shown in Table 1, the leading-edge radius on the F/A-18E is smaller than that on the F/A-18C. Two different configurations were analyzed to determine the effect of leading-edge radius. These cases correspond to morphing cases 5 and 10 in Figure 7. In the first case, the leading-edge radius of the F/A-18C was reduced to match that of the F/A-18E. In the second case, a leading-edge snag was added to the F/A-18C while reducing the leading-edge radius of the wing. The WRBM coefficient for both cases is shown in Figure 25. In this figure, the results from the first case are shown on the top while the results of the second case are shown on the bottom. The plots of WRBM in this figure indicate that reducing the leading-edge radius does not shift the onset AoA. As a result, the reduction of the leading-edge radius does not appear to be a contributing factor to AWS.

Leading-Edge Flap-Chord Ratio

The effect of the leading-edge flap-chord ratio on abrupt stall was also investigated using two different configurations. In the first case, the hinge line on the F/A-18C was moved from 20% chord to 11.3% chord. This was accomplished without changing the planform shape of the F/A-18C. The planform of the F/A-18C wing with reduced leading-edge flap-chord ratio is compared to the F/A-18C wing in Figure 11. The F/A-18C wing with reduced leading-edge flap-chord ratio is shown in the upper-right corner of the figure. A flap-chord ratio of 11.3% was chosen since the flap-chord ratio on the F/A-18E immediately inboard of the snag is 11.3%. This represents the smallest leading-edge flap-chord ratio on the F/A-18E.

In Figure 26, the WRBM for this case is compared to that of the F/A-18C for Mach 0.8 and 0.9. At both Mach numbers, the onset AoA is reduced by 1 degree as a result of the reduction in leading-edge flap-chord ratio. The change in slope is very distinguishable at Mach 0.9, whereas at Mach 0.8 the slope change is less apparent.

In Figure 27, the WRBM curve and $dc_l/d\alpha$ for the F/A-18C with 11.3% leading-edge flap-chord ratio are plotted at Mach 0.8. The $dc_l/d\alpha$ plot indicates that the most lift is lost between 9 and 10 degrees AoA. This is consistent with the fact that the change in slope of the WRBM curve occurs at 9 degrees AoA. Furthermore, the minimum values of $dc_l/d\alpha$ at 8.5 and 9.5 degrees are similar since the WRBM curve is relatively smooth between 8 and 10 degrees AoA. This further indicates that the $dc_l/d\alpha$ plots can indicate the severity of the abrupt stall shown by the WRBM curves.

The pressure contours, surface-restricted particle traces and regions of flow reversal of the F/A-18C with reduced leading-edge flap-chord ratio are compared to those of the F/A-18C at Mach 0.8 in Figure 28. The flow separation on the wing with reduced leading-edge flap-chord ratio moves rapidly to the leading edge between 9 and 10 degrees AoA. The flow separation on the F/A-

18C between 8 and 10 degrees AoA is gradually moving forward and still has not reached the leading edge at 10 degrees.

In the second configuration, the leading-edge flap of the F/A-18C was modified to include a snag and change the leading-edge flap-chord ratio simultaneously. This results in a wing with a tapered leading-edge flap. The planform of the F/A-18C wing with a snag and tapered leading-edge flap is shown in the lower-right corner of Figure 11. The snag was once again placed at the same non-dimensional spanwise location as it is on the F/A-18E. The leading-edge flap was modified so that the flap-chord ratio immediately inboard of the snag is 11.3%, just as it is on the F/A-18E. Also, the ratio of the chord length between the airfoil section outboard of the snag and inboard of the snag reflects that on the F/A-18E. At the root and tip of the wing, the leading-edge flap-chord ratio is 20%, which is unchanged from the F/A-18C.

To show the effect of leading-edge flap-chord ratio on a wing with a snag, the WRBM coefficients for the F/A-18C wing with a snag and tapered leading-edge flap are compared to those of the F/A-18C with a snag at Mach 0.8 and 0.9 in Figure 29. In this figure, one can see that the onset AoA is reduced by 1.5 degrees at Mach 0.8 and 1.2 degrees at Mach 0.9 when the leading-edge flap-chord ratio is reduced to 11.3% on the F/A-18C wing with a snag. This implies that when a snag is added to the F/A-18C and the leading-edge flap-chord ratio is reduced simultaneously, the onset AoA is reduced from the F/A-18C by 3.5 degrees at Mach 0.8 and 3.2 degrees at Mach 0.9. Recall from Figure 6 that the onset AoA for the F/A-18C is 10 and 11 degrees AoA at Mach 0.8 and 0.9, respectively. Based on these results, the reduction of the leading-edge flap-chord ratio may be contributing significantly to AWS.

The pressure contours, surface-restricted particle traces and regions of flow reversal of the F/A-18C with a snag and tapered leading-edge flap are compared to those of the F/A-18C with a snag at Mach 0.9 in Figure 30. The flow separation on the wing with a snag and tapered leading-edge flap moves forward at a more rapid rate between 7 and 9 degrees than it does on the F/A-18C wing with a snag. This rapid movement of the flow separation region causes the slope of the WRBM curve to change sign at 7.8 degrees, as shown in Figure 29.

The sectional lift and $dc_l/d\alpha$ for the F/A-18C, F/A-18C with a snag, F/A-18C with a snag and tapered leading-edge flap and the F/A-18E at Mach 0.9 are shown in Figures 31 and 32, respectively. The largest loss in lift on the F/A-18C with a snag and tapered leading-edge flap occurs between 7.8 and 8.5 degrees AoA, while the largest loss in lift on the F/A-18E occurs between 7.5 and 8 degrees AoA.

As was mentioned above, the reduction of the leading-edge flap-chord ratio may be contributing significantly to AWS. The chordwise pressure distribution shown in Figure 33 gives insight into how the flap-chord ratio is contributing to abrupt stall. In this figure, a comparison is made between the chordwise pressures on the F/A-18C and the F/A-18C with 11.3% leading-edge flap-chord ratio. Recall from Table 1 that the F/A-18C has a leading-edge flap-chord ratio of 20%. In Figure 33, on the upper surface the flow decelerates on the leading-edge flap from the leading edge to the hinge line. When the length of the leading-edge flap is reduced, the flow has less length to decelerate and, as a result, is moving faster when it encounters the hinge line. The faster velocity upstream of the hinge line accelerates around the hinge line. As a result of the reduced leading-edge flap length and increased velocity after the hinge line, shock induced flow separation occurs earlier on the wing.

Summary of Results

The difference between the onset AoA of each morphing configuration and the baseline F/A-18C is shown in Table 2 for Mach 0.8 and 0.9. The results in this figure were used to determine that the camber may be contributing to the abrupt stall encountered by the pre-production F/A-18E, while the snag and leading-edge flap-chord ratio may be contributing significantly to the abrupt stall.

Since the addition of the leading-edge snag to the F/A-18C wing reduced the onset AoA of AWS by 2 degrees, the addition of the snag was determined to be a significant contributor to the abrupt stall. The question used to determine whether the other five wing parameters were contributing to abrupt stall was: “When the wing

parameter is modified in combination with a leading-edge snag, is the onset AoA reduced beyond that of the F/A-18C with a snag?" If the answer to this question was "Yes", then the wing parameter was considered to be contributing to the abrupt stall. The only two wing parameters that fall into this category were the camber and leading-edge flap-chord ratio.

When adding a leading-edge snag to the F/A-18C wing and reducing the leading-edge flap-chord ratio, the onset AoA is reduced by 3.5 degrees at Mach 0.8 and 3.2 degrees at Mach 0.9. The WRBM is plotted as a function of AoA for the F/A-18C, F/A-18C with a snag, F/A-18C with a snag and tapered leading-edge flap and the F/A-18E at Mach 0.9 in Figure 34. This figure clearly shows that by adding a snag to the F/A-18C and reducing the leading-edge flap-chord ratio, the WRBM curve resembles that of the F/A-18E. The onset AoA is 7.8 degrees for the F/A-18C with a snag and tapered leading-edge flap and 7.5 degrees for the F/A-18E. This figure re-emphasizes that the snag and leading-edge flap-chord ratio are determined to be the major geometric contributors to the abrupt stall on the F/A-18E.

Concluding Remarks

Several wing parameters on the F/A-18C wing have been modified to reflect the changes incorporated in the design of the pre-production F/A-18E. This effort was undertaken as part of the AWS program to determine the wing parameters that contributed to the abrupt stall type characteristics initially encountered by the pre-production F/A-18E during flight tests. The knowledge gained from this research could be used by designers of future aircraft to avoid AWS.

The effects of thickness, camber, twist, leading-edge radius, leading-edge flap-chord ratio and a leading-edge snag on abrupt stall were studied during this project using eleven different morphed configurations. The WRBM coefficient was plotted as a function of AoA to determine which wing parameters contributed to AWS on the F/A-18E. Two cases clearly indicate that smaller increments in AoA may be necessary when using the WRBM curve to determine the onset AoA.

The results of this research indicate that the addition of a leading-edge snag and the reduction of the leading-edge flap-chord ratio are the primary contributors to AWS. In addition, the removal of the camber from the wing may also be contributing to the abrupt stall. The thickness, twist and leading-edge radius, however, do not appear to be contributing to the abrupt stall.

The derivative of the sectional lift coefficient with respect to AoA was also investigated during this research as a potential FOM. Although it was not used as a FOM, there is good correlation between the AoA where the largest loss in lift occurs on the wing and the onset AoA from the WRBM curves. The derivative of sectional lift also indicates the spanwise location where lift is being lost. Furthermore, the derivative of sectional lift with AoA also illustrates a larger lift loss on the wing when the slope of the WRBM curve changes more abruptly. Additional research is needed to determine whether the derivative of sectional lift with respect to AoA can be used as a reliable FOM for lateral activity for future programs.

Acknowledgements

The authors wish to acknowledge Dr. Shawn Woodson, Mr. Joe Laiosa and Mr. Darren Grove of NAVAIR and the other members of the AWS Program for their guidance during this project. Also, the authors wish to acknowledge the Department of Defense High Performance Computing Modernization Program for providing the computer resources necessary to perform this task. Specifically, the machines at the U.S. Army Engineering Research and Development Center, Army Research Laboratory, Aeronautical Systems Center, Naval Research Laboratory, and Space and Missile Defense Command were invaluable.

References

1. Grove, D.V.; Laiosa, J.P.; Woodson, S.H.; Stookesberry, D.C.: "Computational Fluid Dynamics Study of an Abrupt Wing Stall Phenomena on the F/A-18E," AIAA-2002-1025, January 2002.

2. Hall, R.M.; Woodson, S.H.: "Introduction to the Abrupt Wing Stall (AWS) Program," AIAA-2003-0589, January 2003.

3. Lamar, J.E.; Hall, R.M.: "AWS Figure of Merit (FOM) Developed Parameters from Static Tests," AIAA-2003-0745, January 2003.

4. Bush, R.H.; Tower, G.D.; Towne, C.E.: "WIND: The Production Flow Solver of the NPARC Alliance," AIAA-1998-0935, January 1998.

5. Menter, F.R.: "Zonal Two Equation k-ω Turbulence Models for Aerodynamic Flows," AIAA-1993-2906, 1993.

Figures

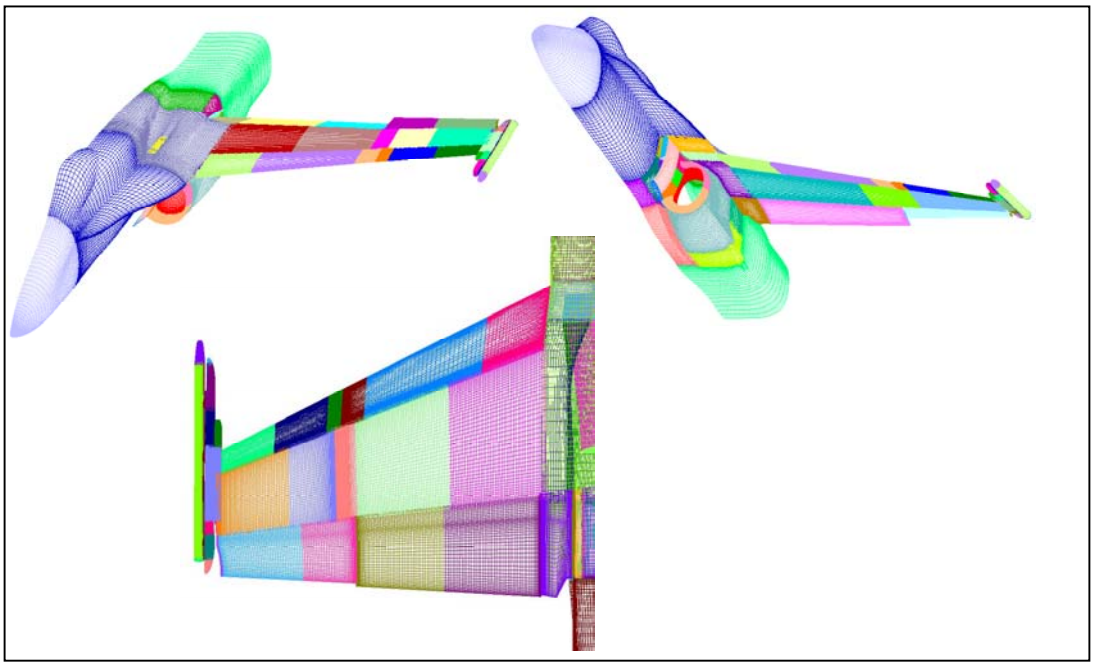

Figure 1. The F/A-18C computational grid

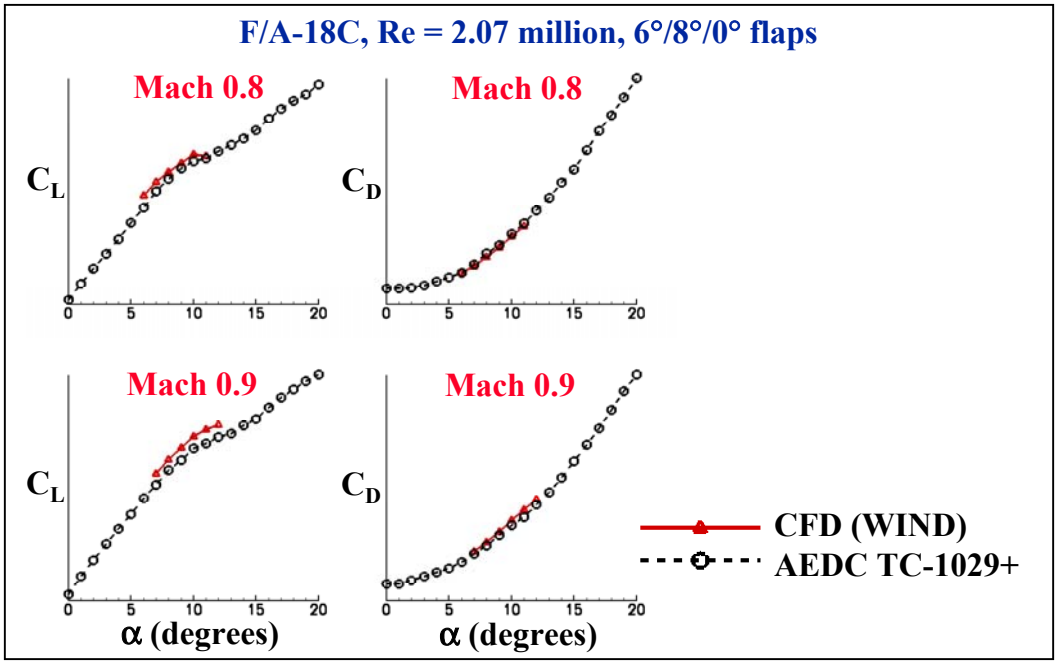

Figure 2. Comparison of aircraft lift and drag coefficients between CFD and wind-tunnel experiment

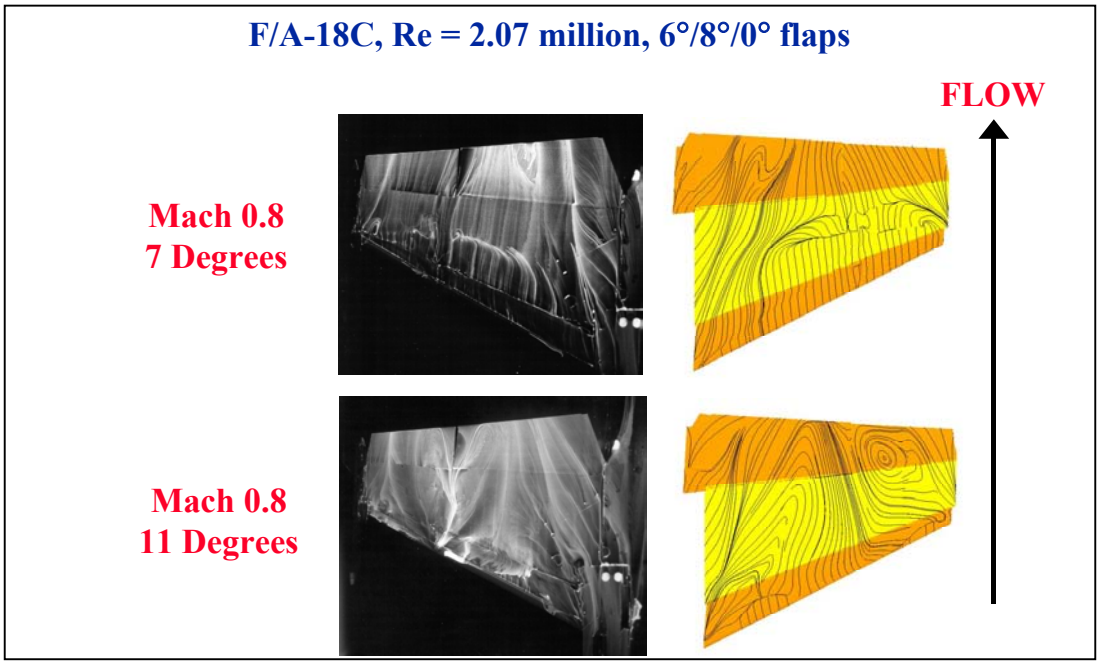

Figure 3. Comparison of CFD surface-restricted particle traces and wind-tunnel oil flow images

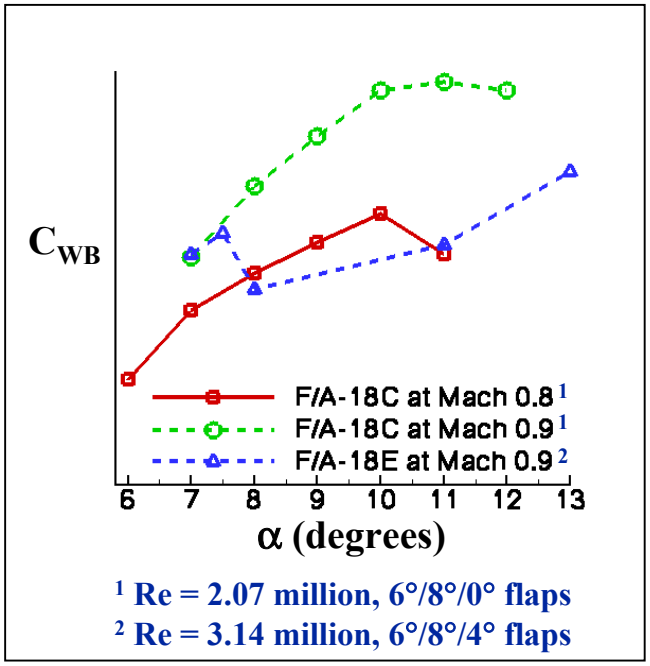

Figure 4. WRBM coefficient versus AoA as a Figure of Merit

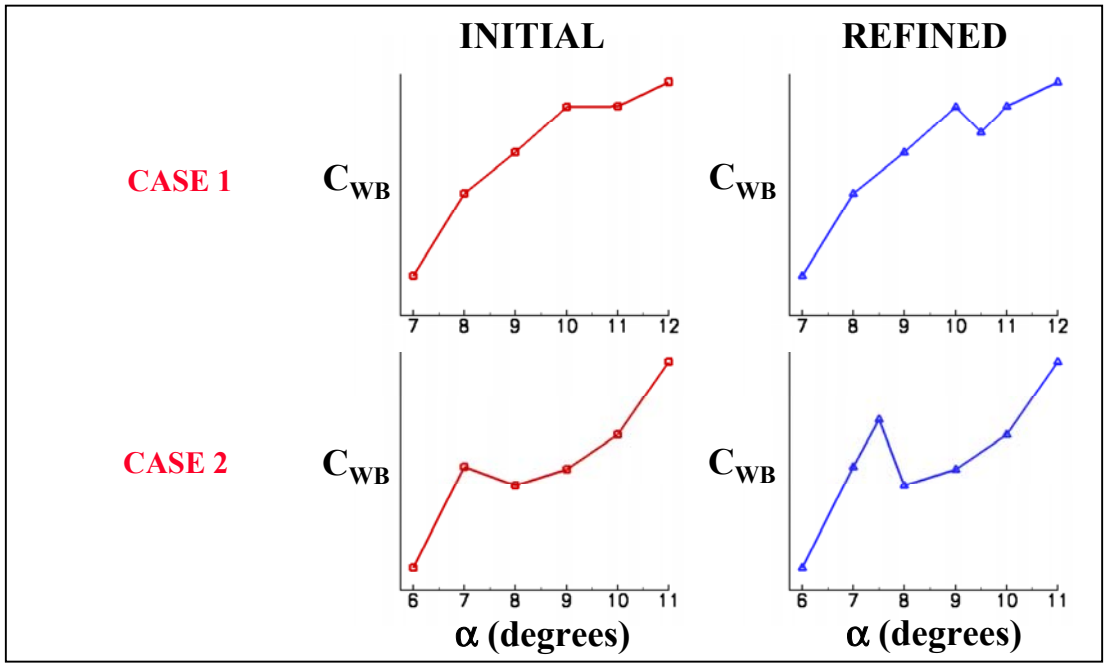

Figure 5. The effect of smaller AoA increments on the WRBM curve

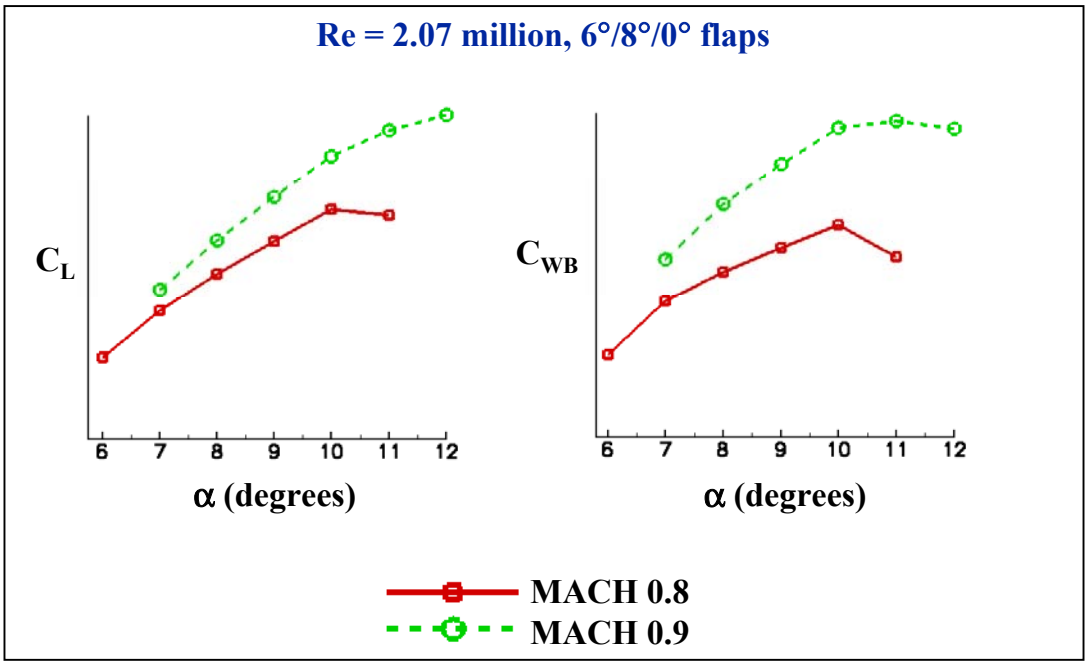

Figure 6. Lift and WRBM coefficients versus AoA for the F/A-18C

Wing Parameters	Morphing Case										
	1	2	3	4	5	6	7	8	9	10	11
Snag	X						X	X	X	X	X
Thickness		X					X				
Camber			X					X			
Twist				X					X		
LE radius					X					X	
LE flap-chord ratio						X					X

Figure 7. The morphing configurations used during this research

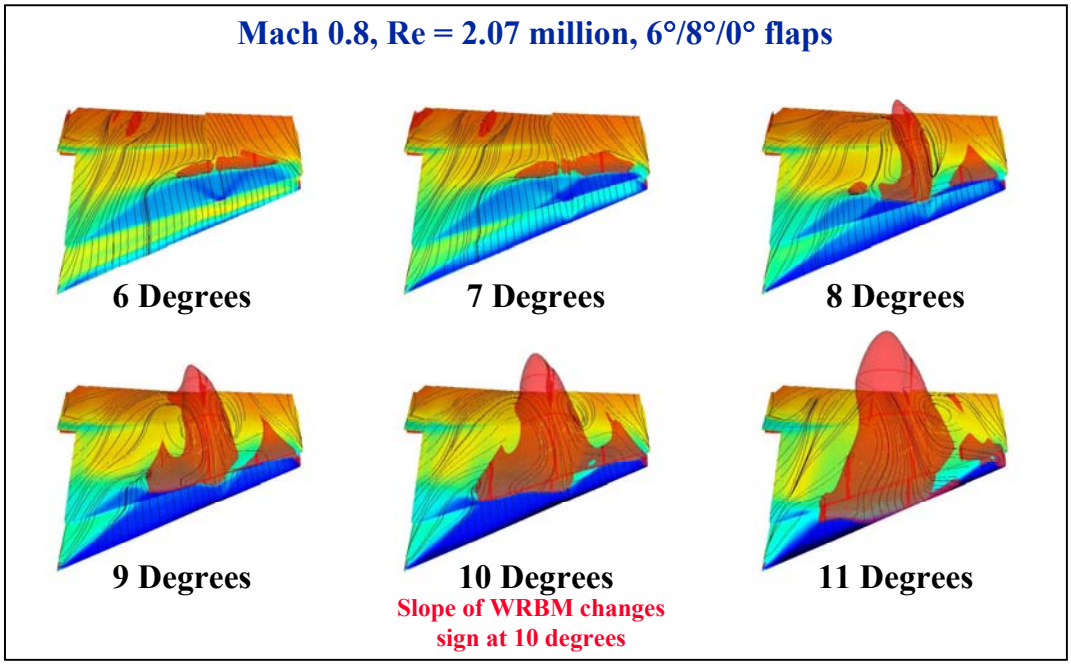

Figure 8. Pressures, surface-restricted particle traces and regions of off-body flow reversal for the F/A-18C at Mach 0.8

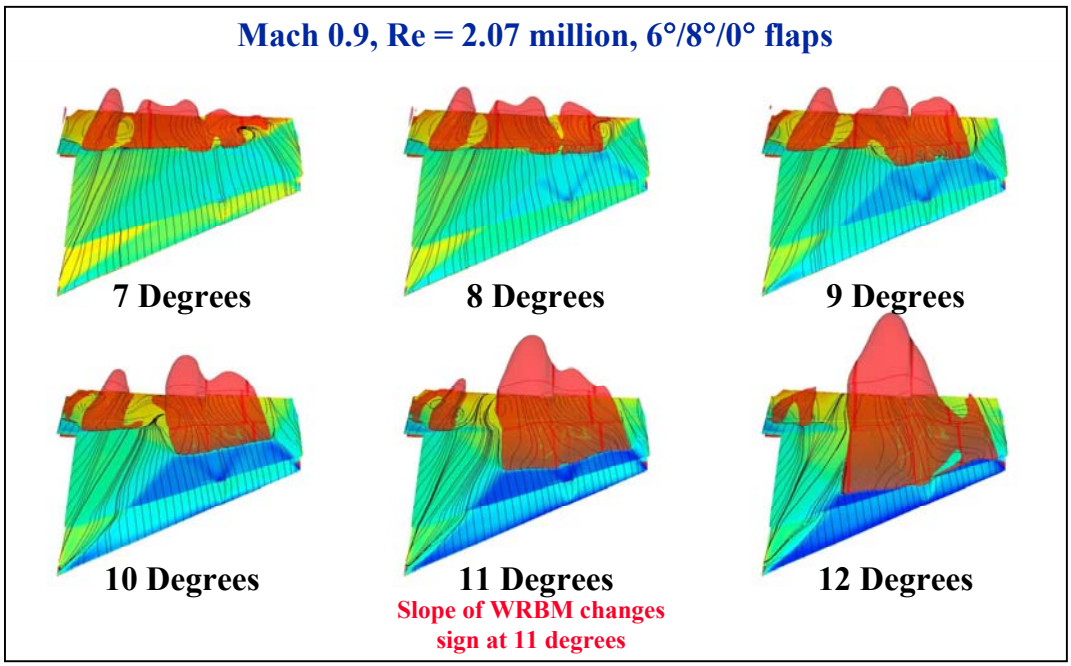

Figure 9. Pressures, surface-restricted particle traces and regions of off-body flow reversal for the F/A-18C at Mach 0.9

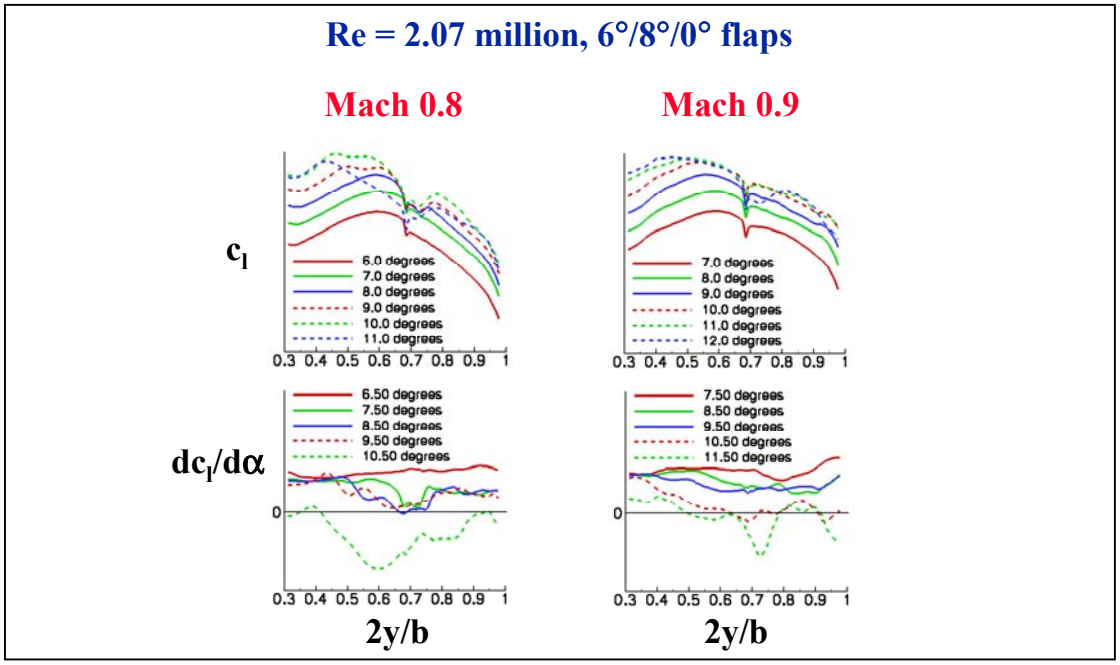

Figure 10. Sectional lift and its derivative with respect to AoA versus spanwise location for the F/A-18C

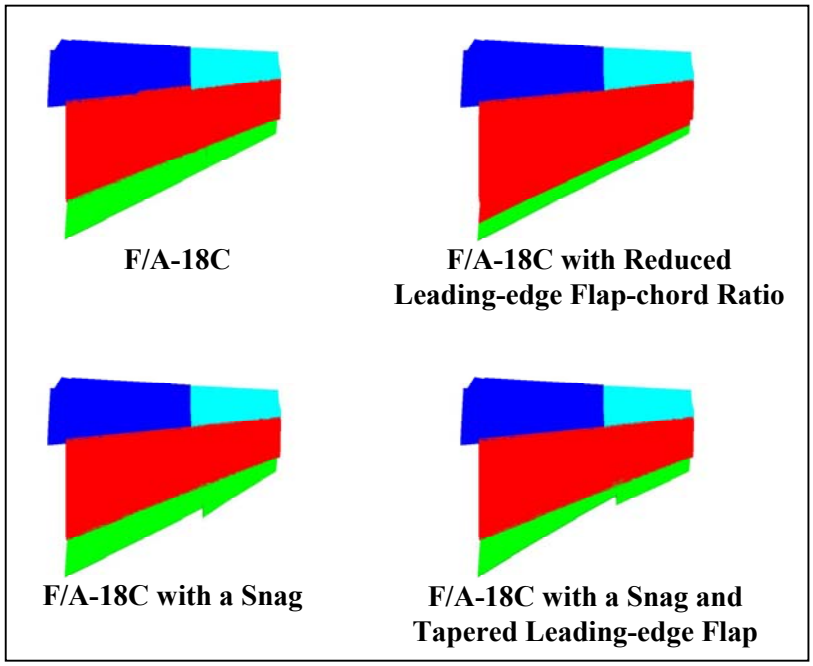

Figure 11. Wing planforms of the F/A-18C, F/A-18C with a snag, F/A-18C with reduced leading-edge flap-chord ratio and the F/A-18C with a snag and tapered leading-edge flap

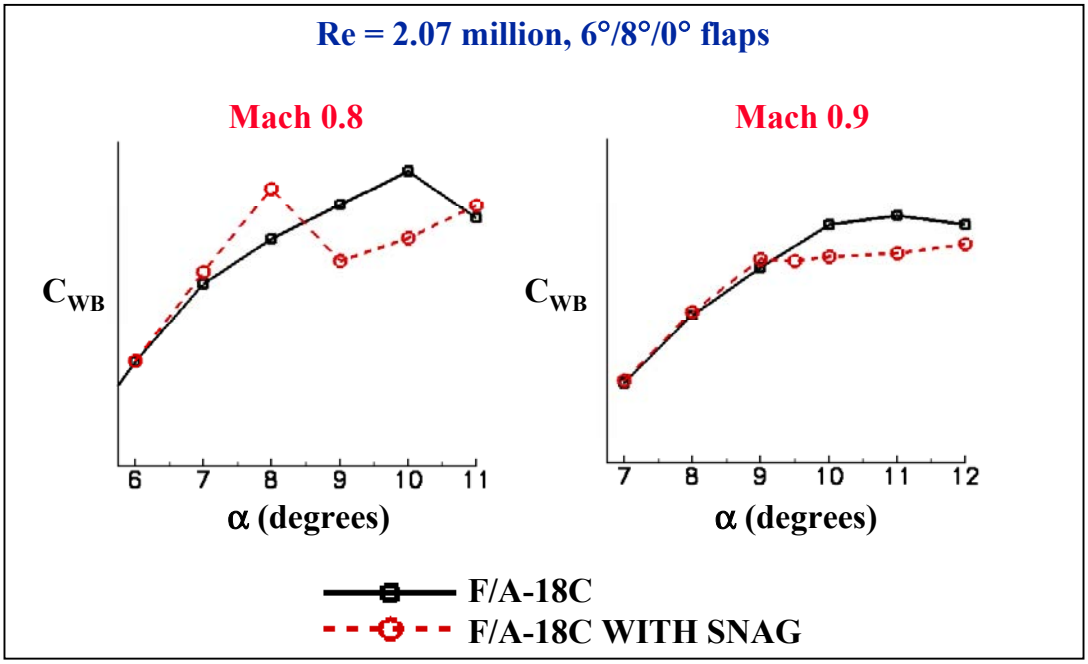

Figure 12. WRBM coefficient versus AoA for the F/A-18C and F/A-18C with a snag

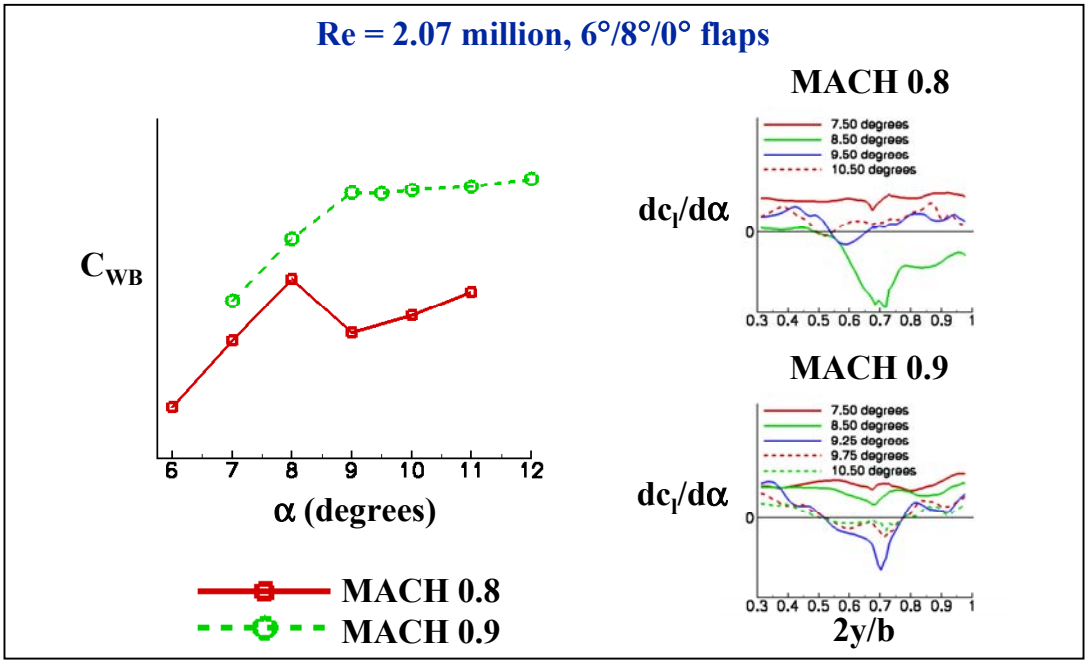

Figure 13. WRBM coefficient versus AoA and derivative of sectional lift coefficient with respect to AoA versus spanwise location for the F/A-18C with a snag

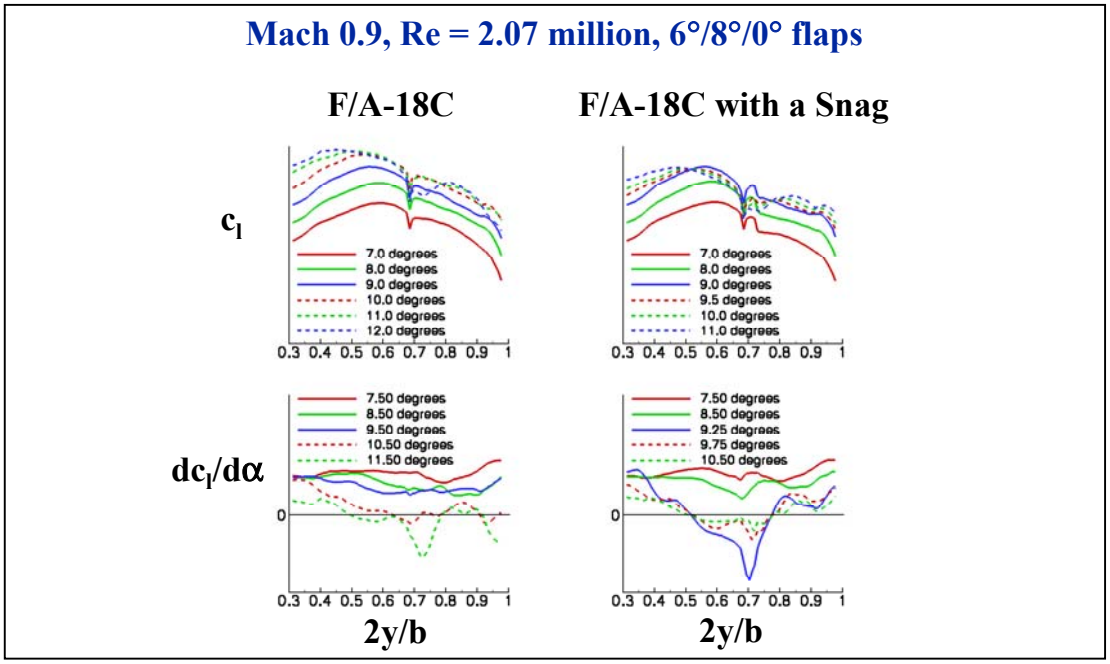

Figure 14. Sectional lift coefficient and its derivative with respect to AoA as a function of spanwise location for the F/A-18C and F/A-18C with a snag

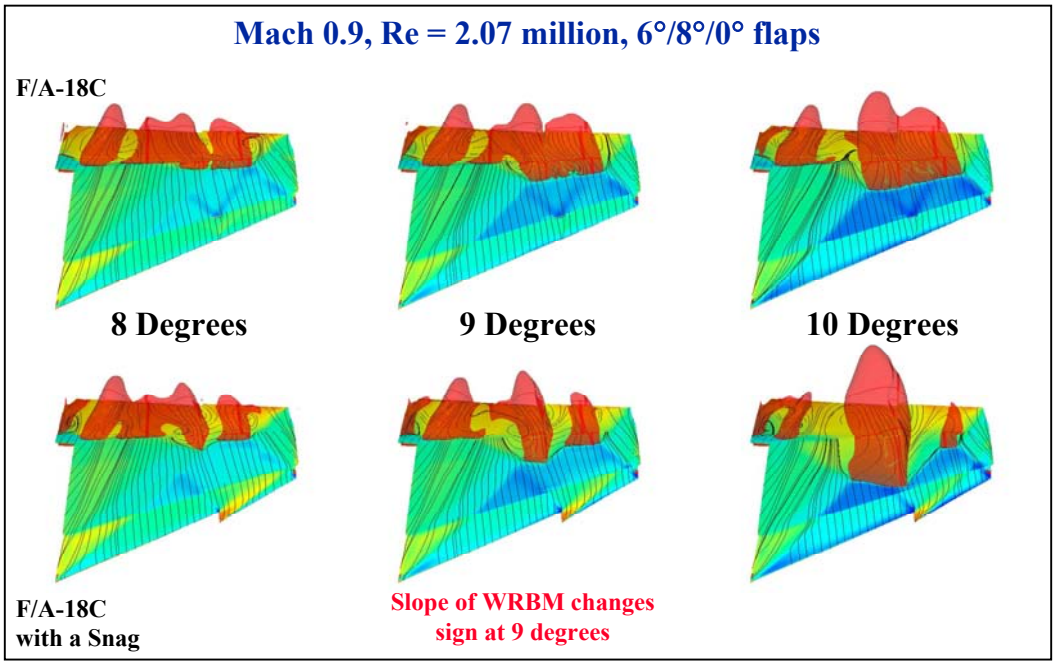

Figure 15. Pressures, surface-restricted particle traces and regions of off-body flow reversal for the F/A-18C and F/A-18C with a snag

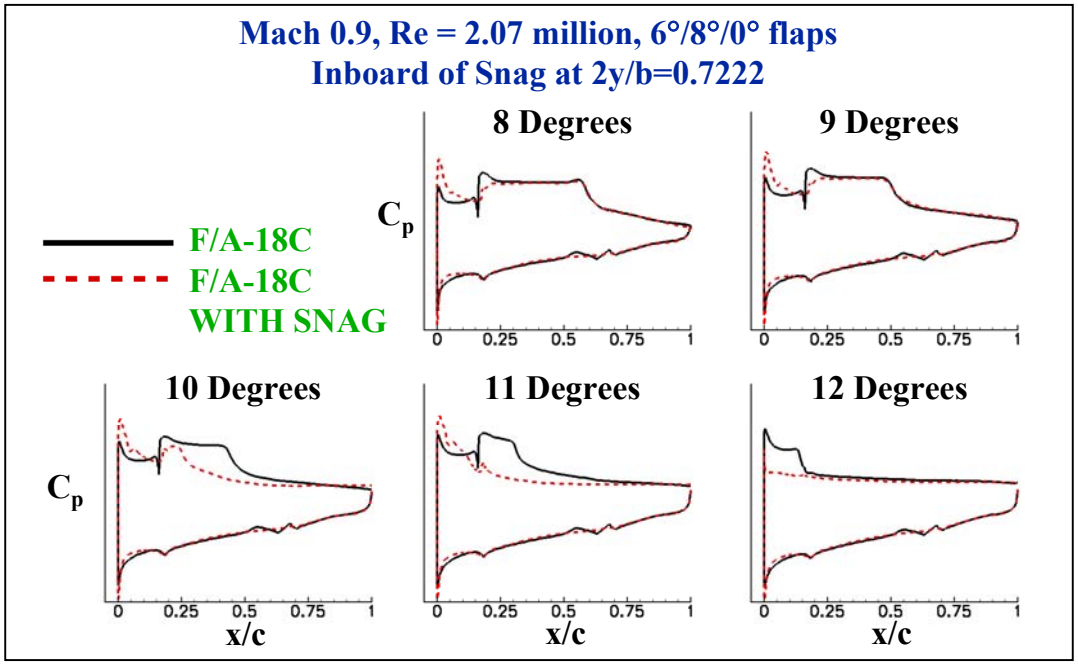

Figure 16. The effect of the snag on the chordwise pressure distribution just inboard of the snag

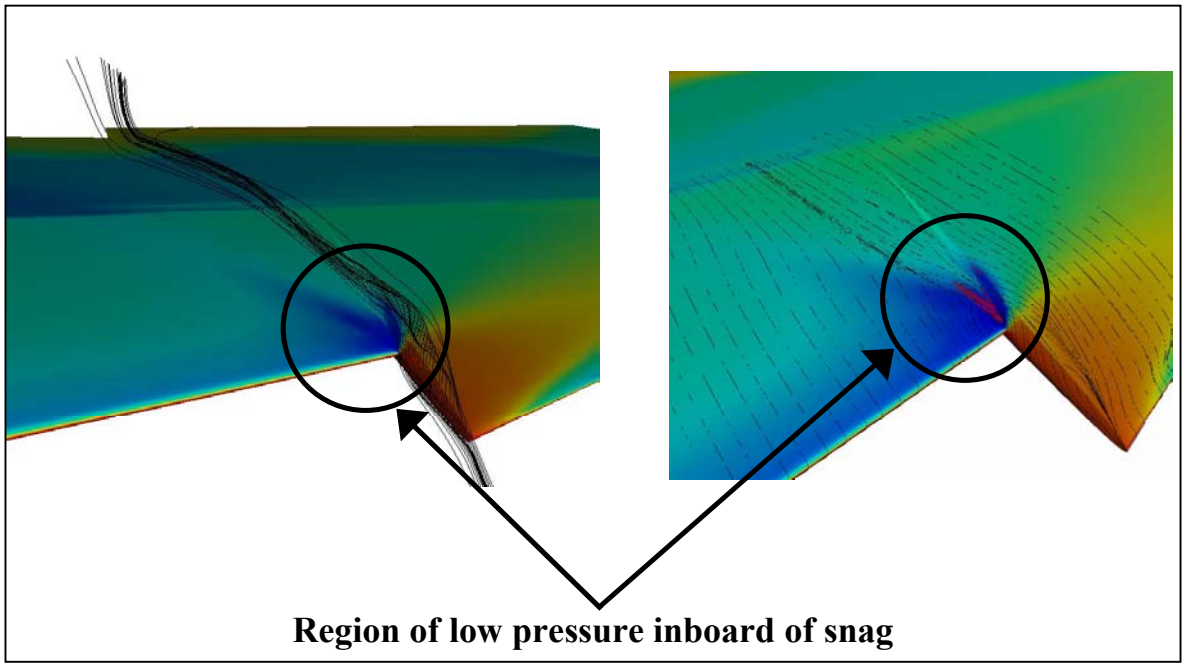

Figure 17. Particle traces near the snag on the F/A-18C with a snag

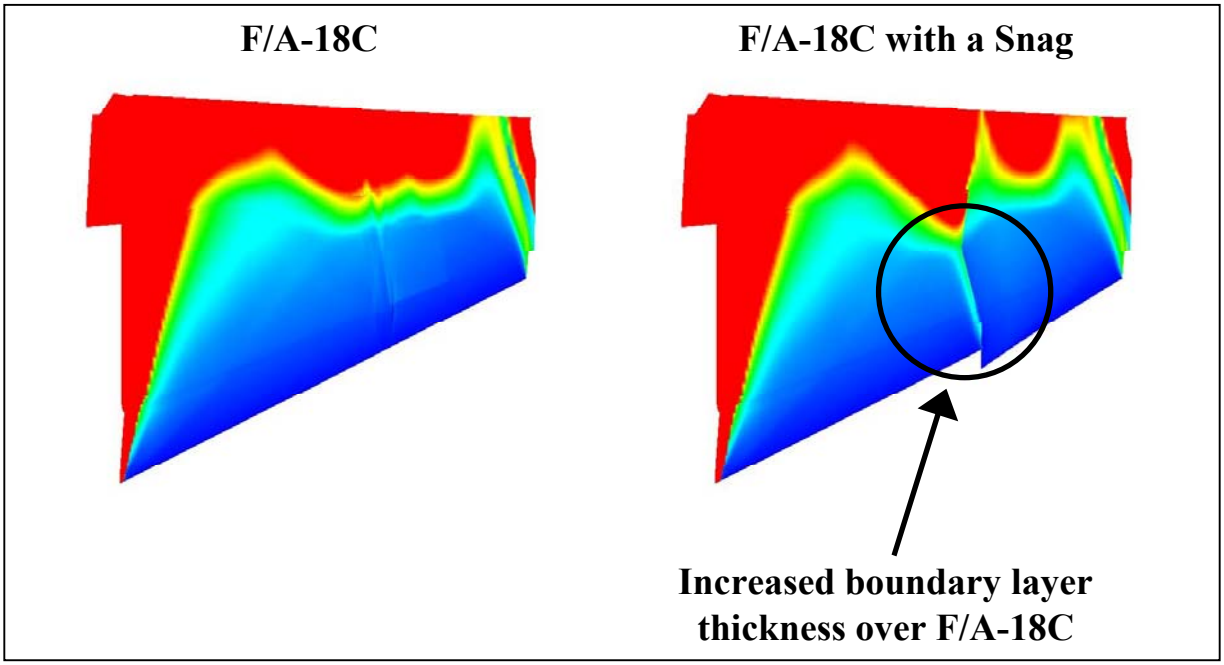

Figure 18. Typical contours of boundary layer thickness on the upper surface of the F/A-18C and F/A-18C with a snag

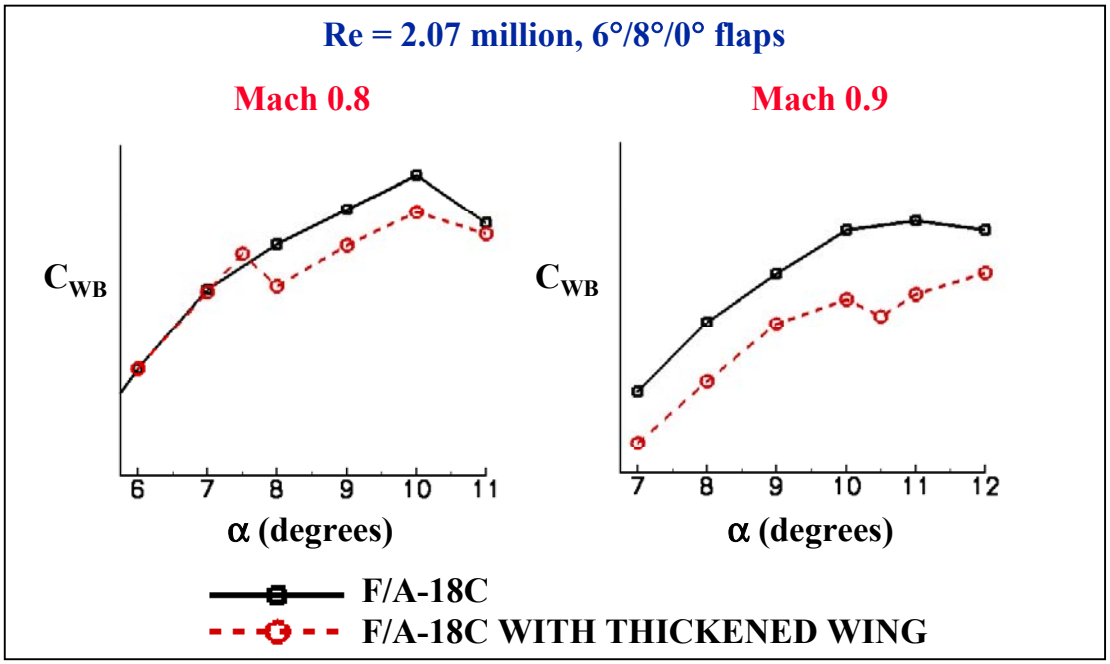

Figure 19. WRBM coefficient versus AoA for the F/A-18C and F/A-18C with a thickened wing

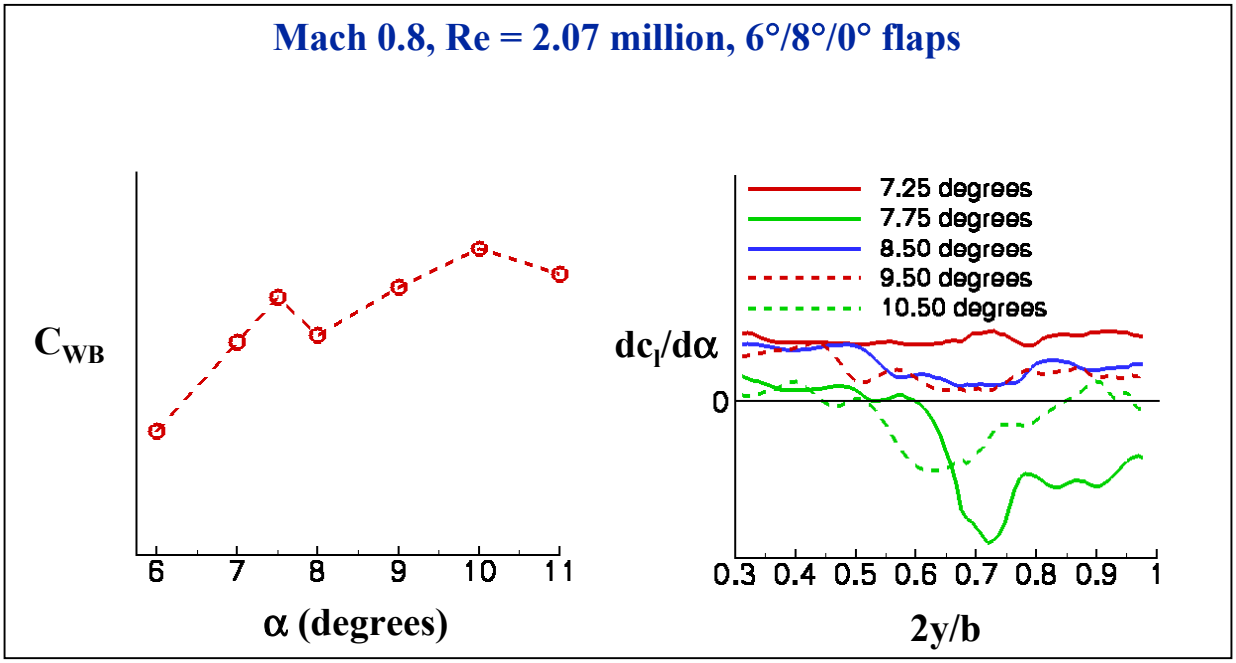

Figure 20. WRBM coefficient versus AoA and the derivative of sectional lift with respect to AoA versus spanwise location for the F/A-18C with a thickened wing

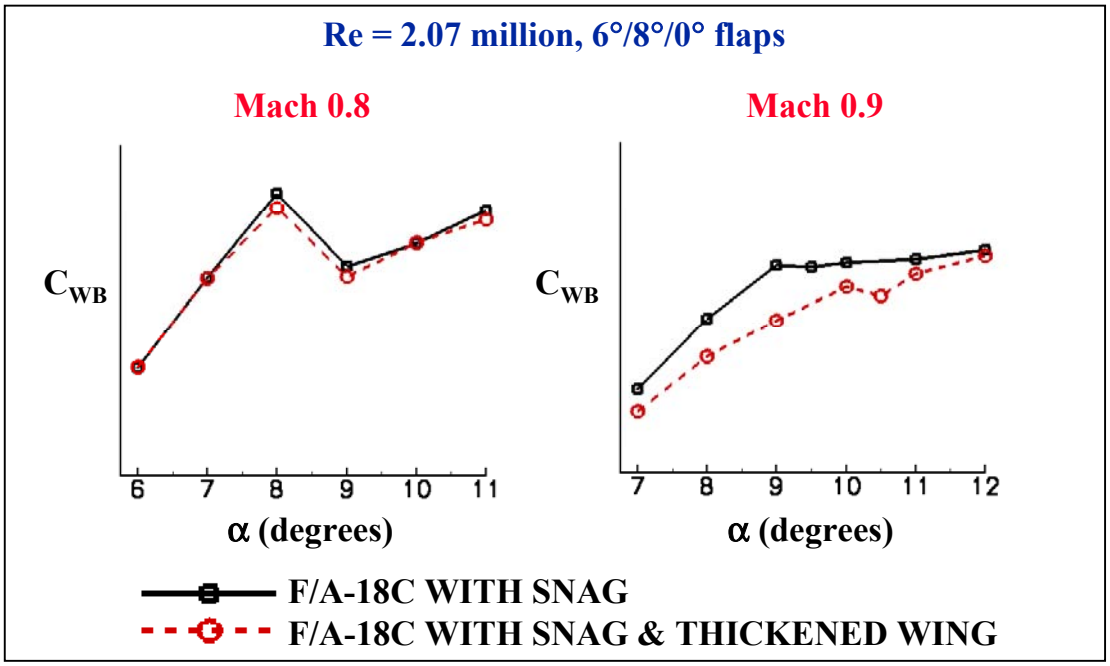

Figure 21. WRBM coefficient versus AoA for the F/A-18C with a snag and F/A-18C with a snag and thickened wing

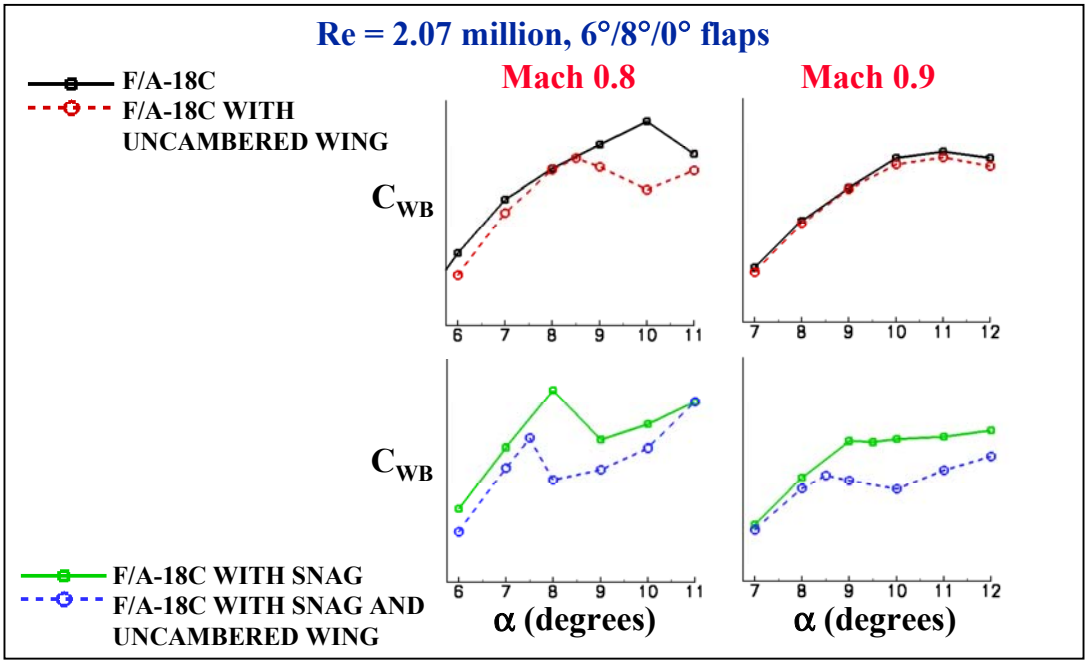

Figure 22. WRBM coefficient versus AoA for the F/A-18C, F/A-18C with an uncambered wing, F/A-18C with a snag and F/A-18C with a snag and uncambered wing

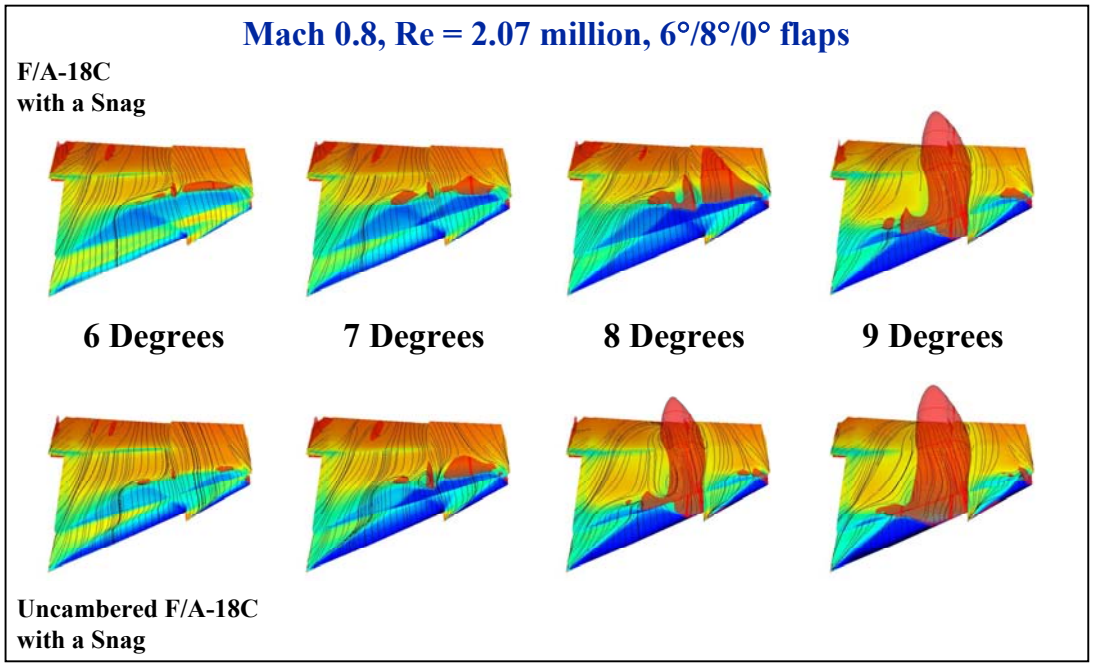

Figure 23. Pressures, surface-restricted particle traces and regions of off-body flow reversal for the F/A-18C with a snag and F/A-18C with a snag and uncambered wing

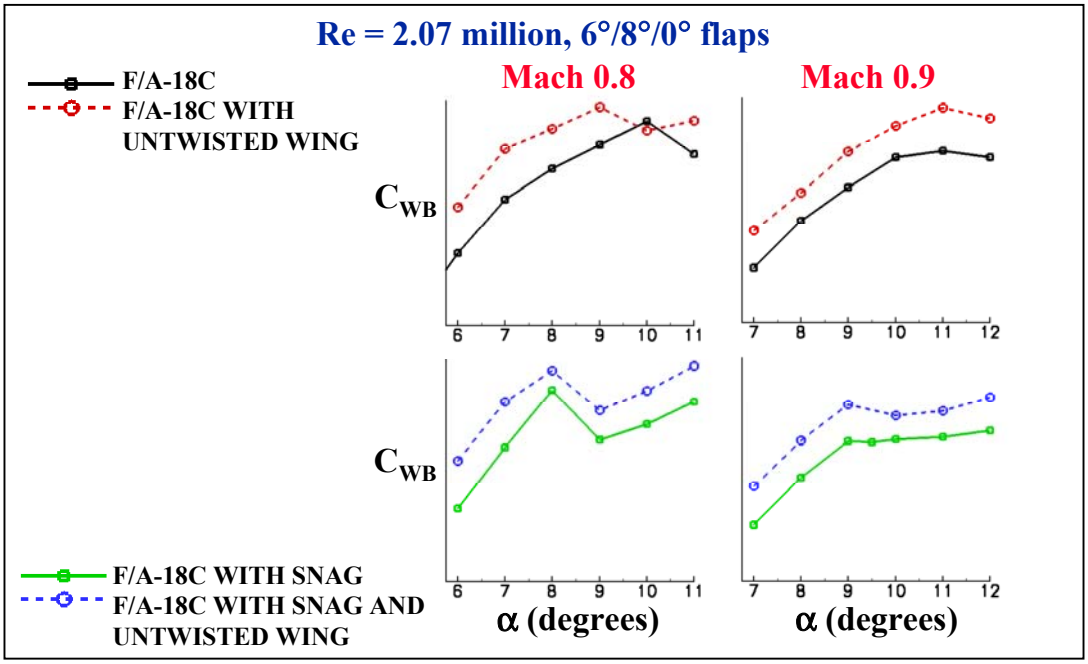

Figure 24. WRBM coefficient versus AoA for the F/A-18C, F/A-18C with an untwisted wing, F/A-18C with a snag and F/A-18C with a snag and untwisted wing

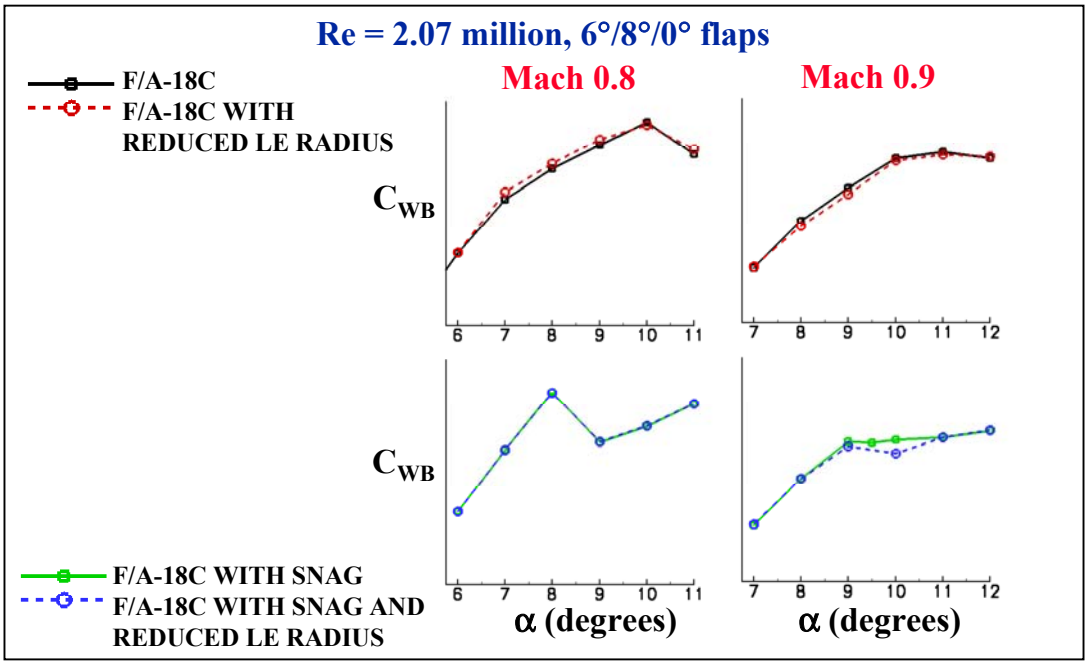

Figure 25. WRBM coefficient versus AoA for the F/A-18C, F/A-18C with reduced leading-edge radius, F/A-18C with a snag and F/A-18C with a snag and reduced leading-edge radius

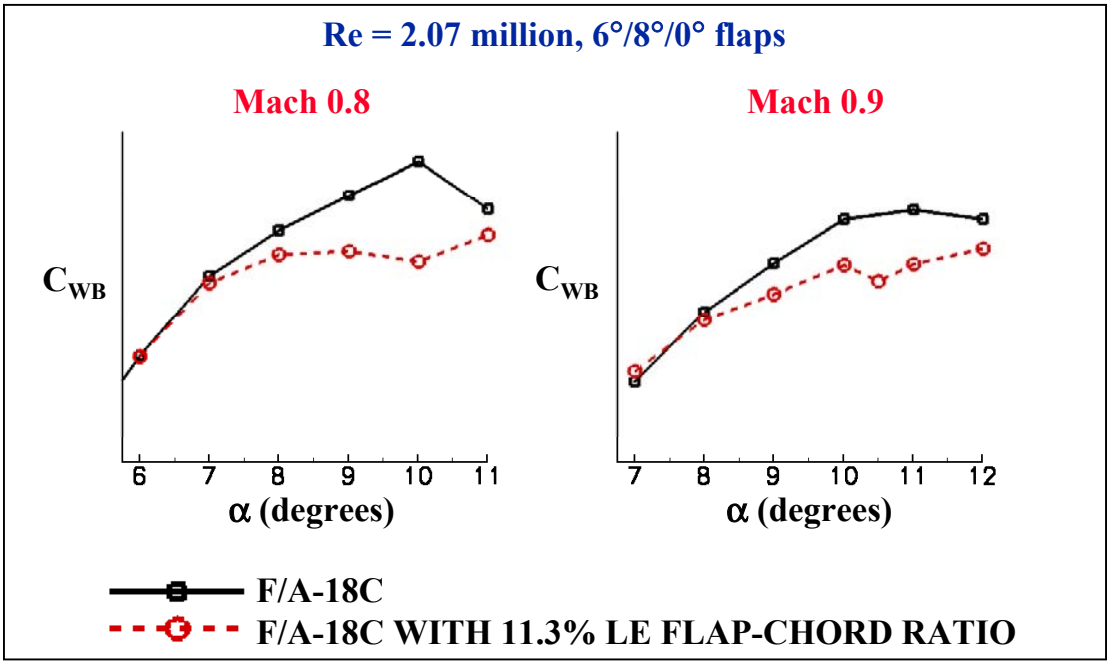

Figure 26. The WRBM coefficient versus AoA for the F/A-18C and F/A-18C with 11.3% leading-edge flap-chord ratio

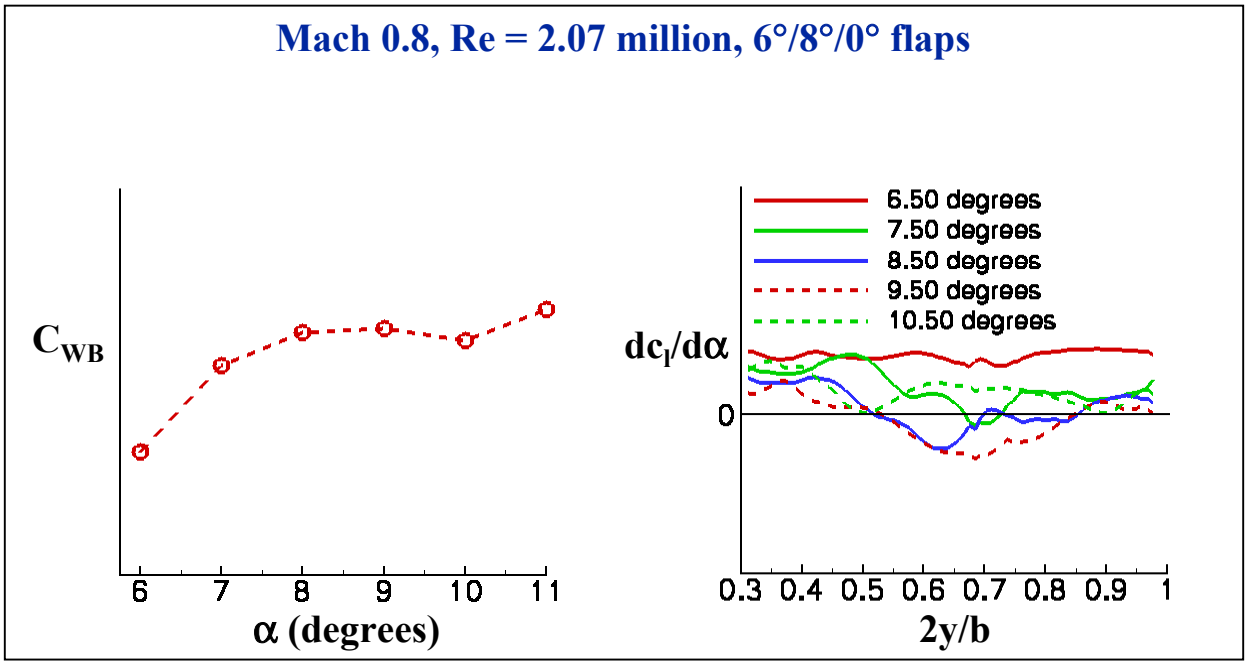

Figure 27. WRBM versus AoA and the derivative of sectional lift coefficient with respect to AoA for the F/A-18C with 11.3% leading-edge flap-chord ratio

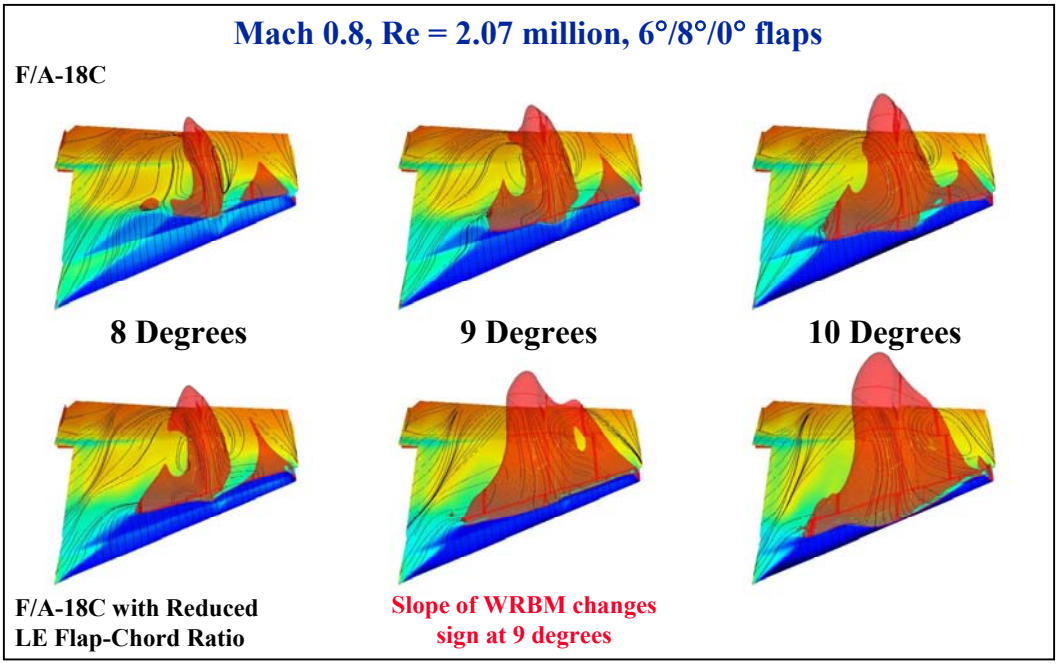

Figure 28. Pressures, surface-restricted particle traces and regions of off-body flow reversal for the F/A-18C and F/A-18C with reduced leading-edge flap-chord ratio

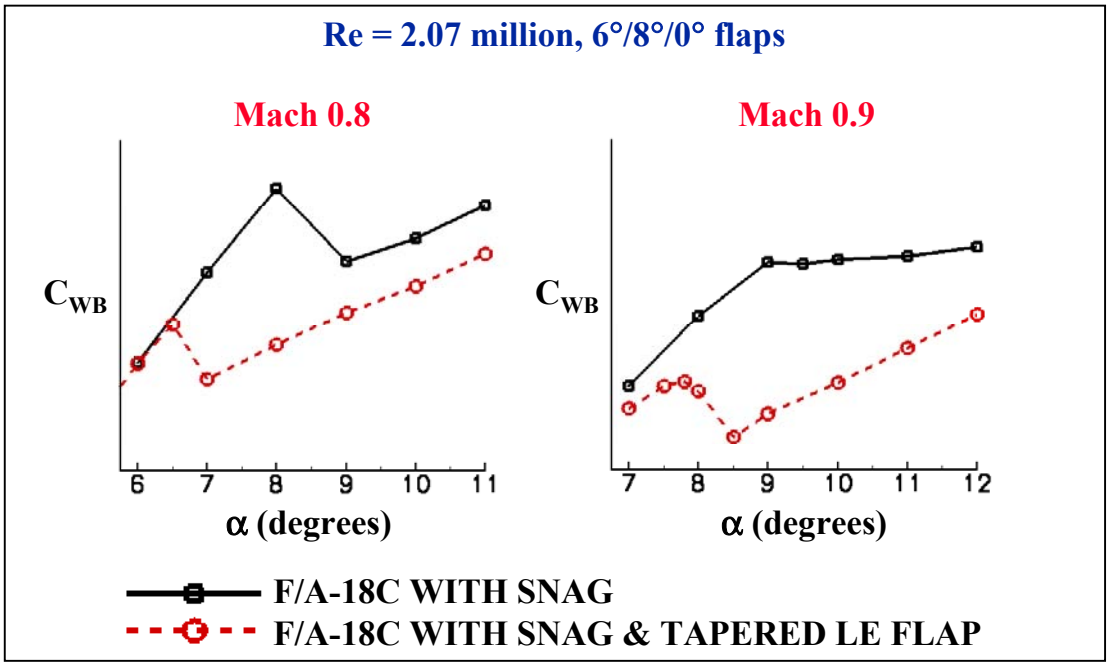

Figure 29. WRBM versus AoA for the F/A-18C with a snag and F/A-18C with a snag and tapered leading-edge flap

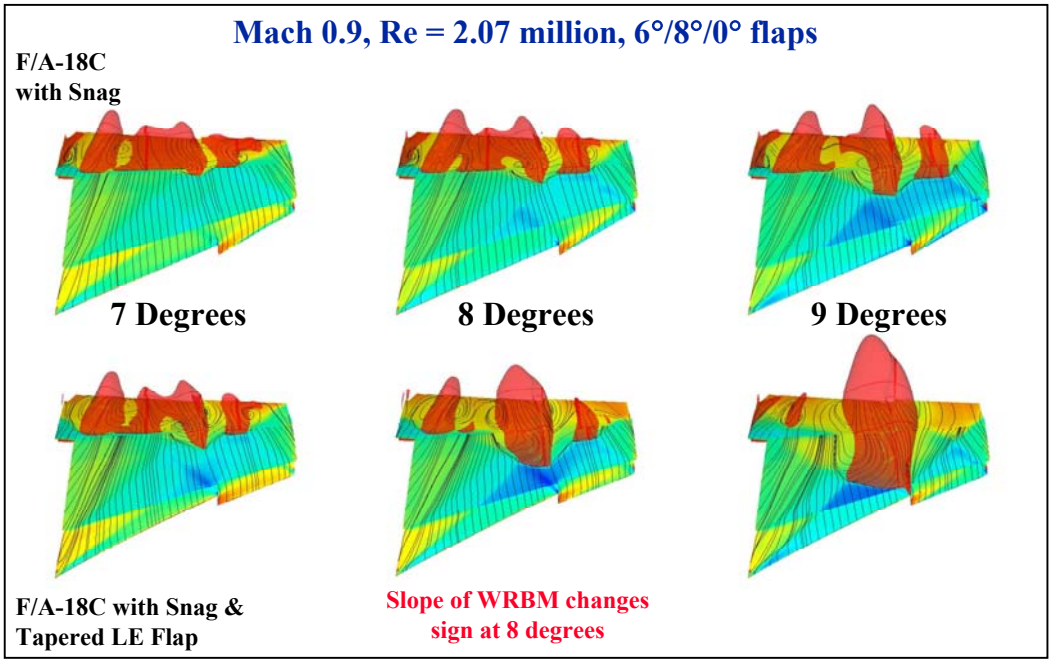

Figure 30. Pressures, surface-restricted particle traces and regions of flow reversal for the F/A-18C with a snag and F/A-18C with a snag and tapered leading-edge flap

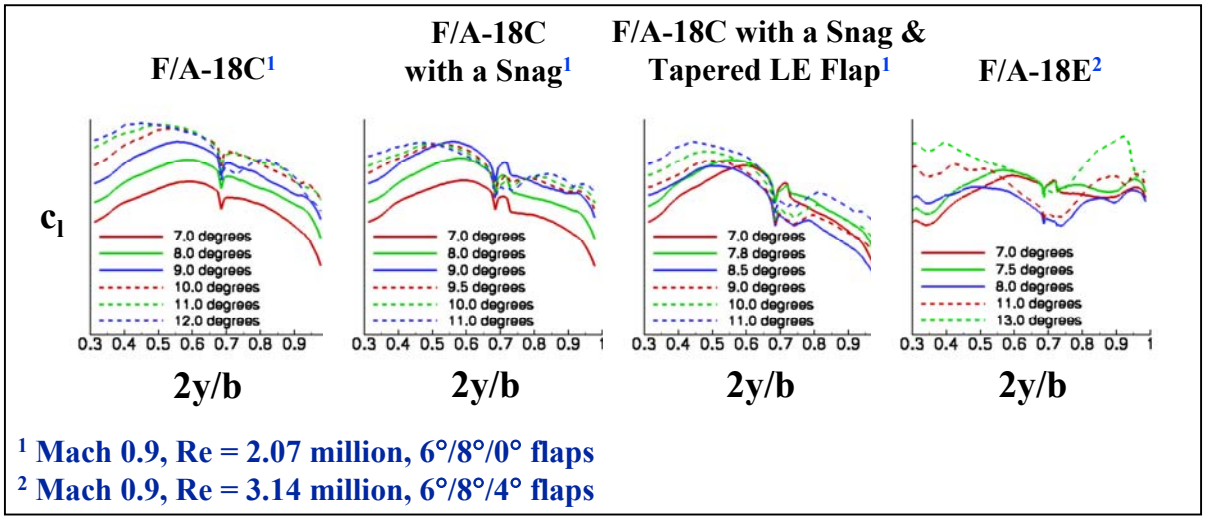

Figure 31. Sectional lift versus spanwise location for the F/A-18C, F/A-18C with a snag, F/A-18C with a snag and tapered leading-edge flap and F/A-18E

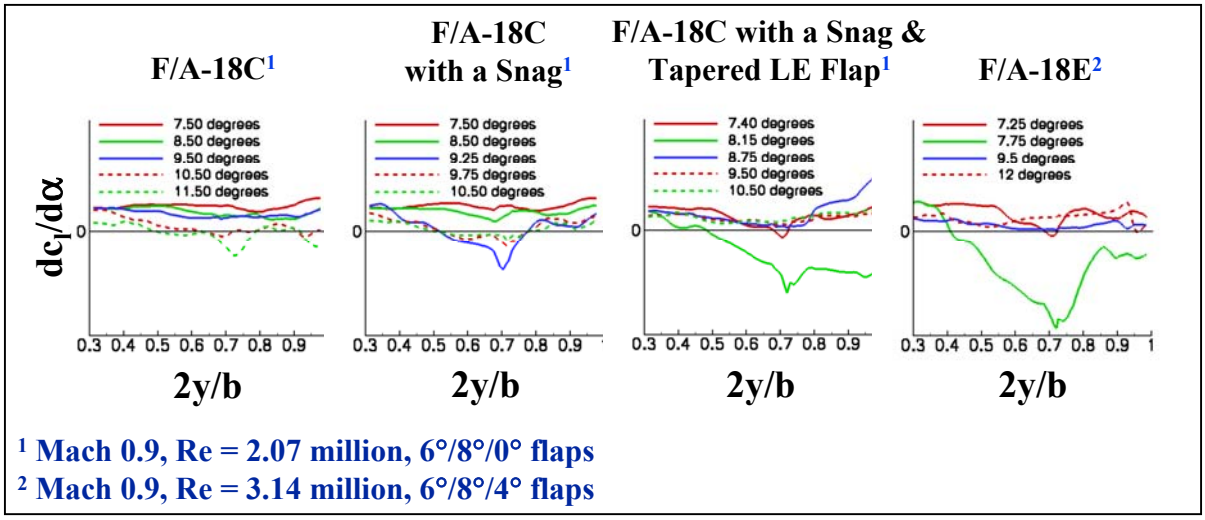

Figure 32. Derivative of sectional lift with respect to AoA versus spanwise location for the F/A-18C, F/A-18C with a snag, F/A-18C with a snag and tapered leading-edge flap and F/A-18E

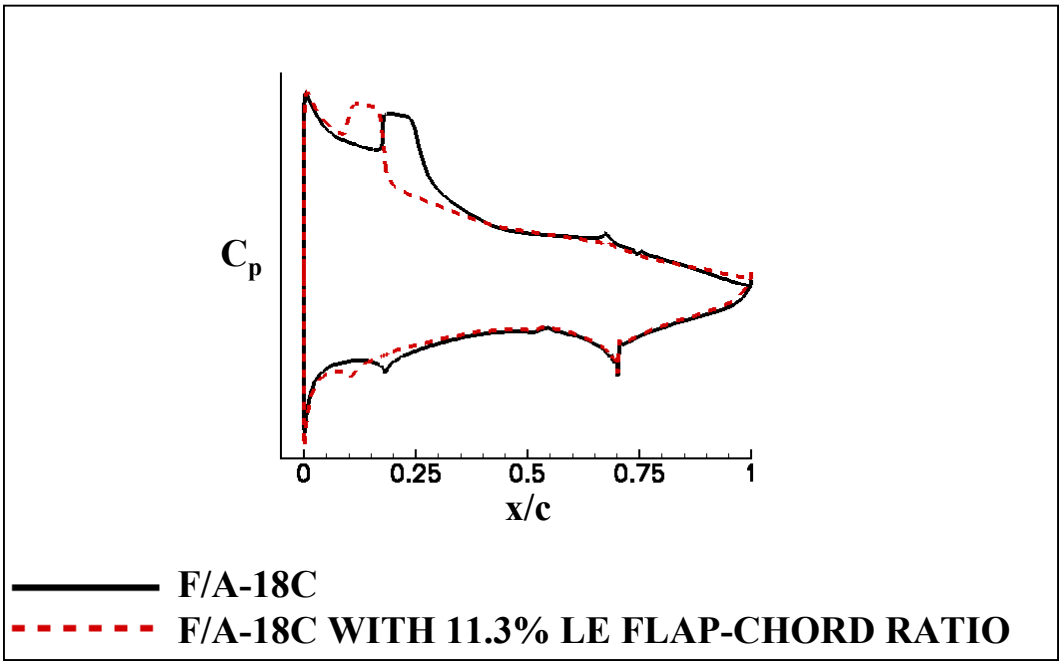

Figure 33. Typical chordwise pressure distribution for the F/A-18C and F/A-18C with 11.3% leading-edge flap-chord ratio

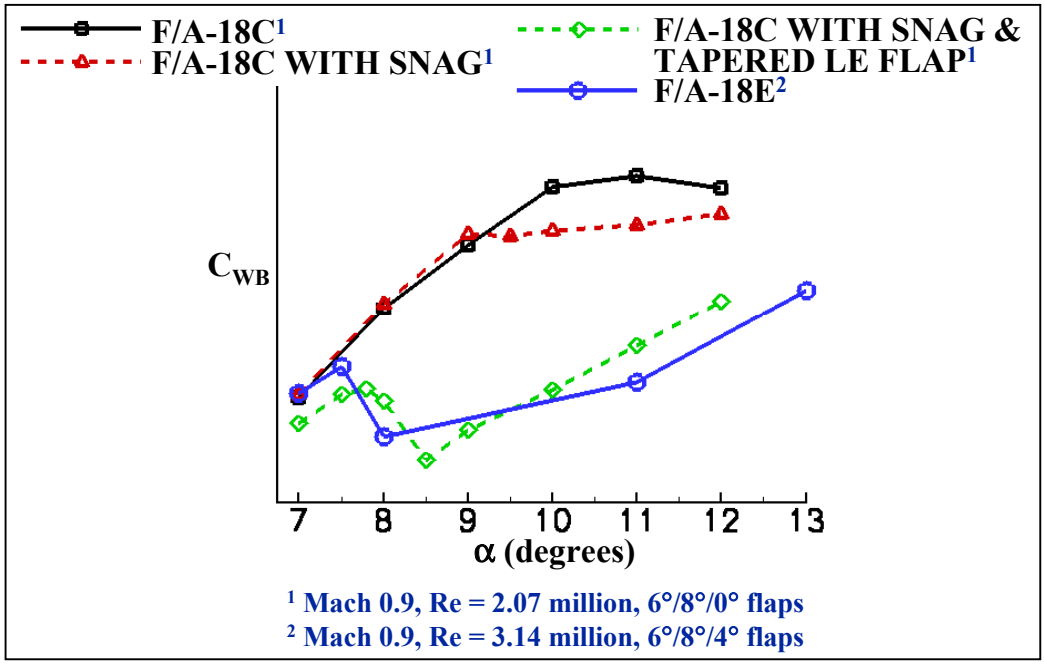

Figure 34. WRBM coefficient versus AoA for the F/A-18C, F/A-18C with a snag, F/A-18C with a snag and tapered leading-edge flap and F/A-18E